



1 **Diurnal, seasonal and long-term behaviours of high Arctic**  
2 **tundra heath ecosystem dynamics inferred from model**  
3 **ensembles constrained by the time-integrated CO<sub>2</sub> fluxes**

4  
5 Wenxin Zhang<sup>1\*</sup>, Per-Erik. Jansson<sup>1</sup> and Bo Elberling<sup>1</sup>

6 <sup>1</sup>Center for Permafrost (CENPERM), Department of Geosciences and Natural Resource Management, University of  
7 Copenhagen, Øster Voldgade 10, DK-1350 Copenhagen, Denmark

8 \*Correspondence to: W. Zhang ([zhang\\_wenxin2005@hotmail.com](mailto:zhang_wenxin2005@hotmail.com))

9 **Abstract**

10 Ecosystem CO<sub>2</sub> fluxes in high Arctic are rather dynamic, as they are sensitive to climatic variability through  
11 multiple ecosystem processes, for instance, vegetation and snow dynamics as well as permafrost thawing, operating  
12 at different time scales. Uncertainties from both high-frequency measurements and model assumptions challenge  
13 model calibration to describe both short- and long-term phenomena related to weather and climate variabilities. In  
14 this study, we generated three model ensembles using a Monte-Carlo based uncertainty approach with acceptance  
15 criteria for 15 years of eddy covariance CO<sub>2</sub> measurements of a high Arctic heath ecosystem based on the time-  
16 integrated CO<sub>2</sub> fluxes within the day, the year and the entire period. The temporal distribution of residuals between  
17 the model and measurements indicated that the three model ensembles reasonably simulated diurnal, seasonal and  
18 long-term behaviours of CO<sub>2</sub> fluxes respectively. The inter-annual variation of CO<sub>2</sub> fluxes over 15 years showed the  
19 current ecosystem is at a transition from being a C sink to a C neutral balance. The long-term behaviour model  
20 ensemble simulated a more intensified diurnal C cycle than the short-term behaviour model ensembles. The  
21 intensified C cycle was mainly attributed to a faster depletion of the soil C pools. The sensitivities of posterior  
22 parameters to the model performance index (coefficient of determination, R<sup>2</sup>) reflected that parameters in the  
23 processes of soil water and heat transfer and snow dynamics regulated the short-term behaviour of CO<sub>2</sub> fluxes, while  
24 parameters in the process of soil decomposition regulated the long-term behaviour of CO<sub>2</sub> fluxes. Our results  
25 suggest that the development of ecosystem models should diagnose their effectiveness in capturing ecosystem CO<sub>2</sub>  
26 exchange behaviour across different time scales. A clear trade-off may exist when the model is tuned to capture both  
27 the short- and long-term variation of CO<sub>2</sub> fluxes. To constrain the model with the time-integrated CO<sub>2</sub> fluxes is a  
28 simple and useful method to reduce the non-explained errors and to identify the crucial link to controlling  
29 parameters and processes.

30 **Keywords:** high Arctic, Greenland, Net ecosystem exchange, Eddy covariance, CoupModel, Monte-Carlo



## 31 1 Introduction

32 Northern permafrost regions characterized by cold climate, short growing seasons and poorly-drained soils with low  
33 fertility hold more than half of global soil carbon (C) with the top 3 m (Hugelius et al., 2014). Currently, widespread  
34 evidence reveals that rapid warming of the Arctic has resulted in permafrost thawing (Grosse et al., 2016). This  
35 implies that further warming can potentially release significant amounts of soil C to the atmosphere, exerting a  
36 positive feedback to global climate change (MacDougall 2012; Koven et al., 2015; Schuur et al., 2009, 2015). On  
37 the other hand, enhanced warming and redistributed wetting may alter growing season length, vegetation phenology  
38 and nutrient and water availability to conditions favored by shrubby and productive ecosystems, which may  
39 sequester more carbon dioxide (CO<sub>2</sub>) comparing to present tundra ecosystems (Xia et al., 2017; Zhang et al., 2013a,  
40 b, 2014; Elmendorf et al., 2012; Myers-Smith et al., 2015). These two opposing ecosystem feedbacks pose a  
41 challenge to identify current and future transition of Arctic ecosystems functioning between C sink and source.

42 The net C gain or loss in ecosystems is described by net ecosystem exchange (NEE) of CO<sub>2</sub> between the atmosphere  
43 and biosphere. Its variability is affected by responses of two constituent fluxes (i.e. gross primary production (GPP)  
44 and ecosystem respiration (ER)) to abiotic and biotic drivers across a wide range of time scales (hours to years)  
45 (Richardson et al., 2007; Baldocchi et al., 2017; Wu et al., 2017). Previous studies used models or wavelet spectra  
46 analysis to disentangle the effects of short- and long-term climatic variation on eddy flux variability (Baldocchi et  
47 al., 2001; Braswell et al., 2005; Stoy et al., 2005, 2009, 2013; Richardson et al., 2007). They generally agreed that  
48 climatic variation tightly controls the short-term variation of CO<sub>2</sub> fluxes, and the effects will become progressively  
49 less important at a long term. The intermediate scales of weather patterns, such as freezing events, heat waves or  
50 rain pulses, may influence plant phenology and microbial activities through their effects on soil temperature and soil  
51 moisture (Vargas et al., 2010). Accordingly, the dominant drivers of ecosystem dynamics can shift from physical or  
52 physiological controls to biological responses to climatic variation along multiple temporal scales (Richardson et al.,  
53 2008; William et al., 2009; Wu et al., 2012a; Fig. 1). This transition possibly becomes remarkable in the Arctic  
54 tundra, which has experienced the substantial changes in seasonal climate and thawing depths of permafrost during  
55 the past few decades (AMAP, 2011; Myers-Smith et al., 2015; Schuur et al., 2015).

56 Soil heat and water transfer, snow dynamics, vegetation dynamics, and soil decomposition are major processes to  
57 regulate Arctic ecosystems NEE variation across multiple time scales. Soil heat and water fluxes respond to diurnal  
58 climatic variation instantaneously. *In situ* manipulation experiments, laboratory incubations and modelling studies  
59 show that increased soil temperatures due to the effects of air warming or more efficient snow insulation are primary  
60 abiotic drivers for increased soil effluxes in both growing seasons and cold seasons (Elberling, 2003; Semenchuk et  
61 al., 2016; Webb et al., 2016; Li et al., 2014). Soil moisture is associated with water stress of photosynthesis and  
62 sometimes may become a limiting factor other than soil temperature by determining the form and magnitude of soil  
63 C release to the atmosphere (Blok et al., 2016; Natali et al., 2015). Snow dynamics is another important aspect that  
64 may cause changes in soil temperature, soil moisture, growing season length, and quantity and quality of substrate  
65 (Lund et al., 2012; Grøndahl et al., 2007). Snow directly impacts on the onset of growing seasons but also has carry-  
66 over effects on the summer- and autumn-time CO<sub>2</sub> exchange through soil moisture limitation (Westergaard-Nielesen  
67 et al., 2017). Moreover, increased soil temperature due to a larger winter snow may also affect the nitrogen (N)



68 cycling (Blok et al., 2015). Vegetation dynamics influences C cycle in terms of short- (e.g. photosynthesis and  
69 stomatal controls) and long-term responses (e.g. changes in composition, structure and functioning). Increased soil  
70 decomposition due to permafrost thawing might be linked to a longer time scale of process related to the old C  
71 turnover (Elberling et al., 2013). Given that the high Arctic C balance is highly dependent on the different time scale  
72 of changes in environmental drivers and biotic responses, it is imperative to identify processes controlling variations  
73 in C fluxes within-day, between-days and -years.

74 To partition NEE into GPP and ER often relies on the night-time or daytime fitting function by assuming that in  
75 certain circumstances, the observed CO<sub>2</sub> fluxes only represent one constituent flux (Reichstein et al., 2005; Lasslop  
76 et al., 2010). However, this conventional approach may not be applicable for the high Arctic tundra with 24-hour  
77 light in summer-time. In addition, it may suffer from the following limitations. Firstly, solely using either air  
78 temperature or soil temperature to extrapolate ER may not be appropriate when temperature response function is  
79 differential for respiration components (i.e. autotrophic and heterotrophic respiration). For instance, rhizospheric  
80 respiration sometimes has higher temperature sensitivity (i.e. higher Q<sub>10</sub> values) than heterotrophic respiration  
81 (Gaumont-Guay et al., 2008); secondly, other environmental factors may jointly control respiration processes, for  
82 instance, snow and N cycling (Blok et al., 2015, 2016); last but not the least, confounding effects of abiotic and  
83 biotic factors propagating along the time scale cannot be well represented by the statistical approach (Braswell et al.,  
84 2005; Paschalis et al., 2015). Therefore, ecosystem model is an alternative set of tools to diagnose the C cycling and  
85 project its behaviour at different temporal scales in relation to other ecosystem processes (Stoy et al., 2009). Besides,  
86 posterior parameter distributions and probabilistic ensembles identified by a Monte Carlo-based uncertainty  
87 approach used in the model allow us to explore the most important parameters for C dynamics and the level of their  
88 uncertainties (Prihodko et al., 2008; Dietze et al., 2011).

89 In this study, we used a process-oriented ecosystem model (CoupModel) to simulate 15 years (2000-2014) C  
90 dynamics for a high Arctic tundra heath ecosystem. Seasonal and multi-year eddy covariance fluxes of CO<sub>2</sub> and  
91 surface energy, soil temperature and soil water content were available to evaluate the efficiency of the model. The  
92 main objective of this study was to examine the role of major physical and biological processes regulating the  
93 diurnal, seasonal and long-term variation of CO<sub>2</sub> fluxes and to estimate the ecosystem C budget based on different  
94 temporal (i.e. diurnal, seasonal and long-term) behaviour model ensembles. To enable the modelled CO<sub>2</sub> fluxes to  
95 consistently agree with the observed C flux on describing these temporal behaviours, the calibrated variable used the  
96 NEE integrated for the day, the year and the entire period. To compare time-integrated variables is a simple  
97 approach to examine the balance of mass or the magnification of model-observation residuals. Our specific aims  
98 were (1) to generate three behaviour model ensembles which best describe the diurnal, seasonal and long-term  
99 variation of CO<sub>2</sub> fluxes respectively; (2) to identify relative importance of parameters/processes in simulating  
100 measurement variables; (3) to understand how the differences in the C budgets estimated by the model ensembles  
101 can be explained by the internal C flux rates and the changes in vegetation and soil C pools.



## 102 2 Materials and methods

### 103 2.1 Site description

104 The study site is a *Cassiope tetragona* heath tundra situated at a lower part of Zackenbergdalen in Northeast  
105 Greenland (74°28'N, 20°34'W, 38 m a.s.l.), where the CO<sub>2</sub> flux measurements were collected by an EC mast since  
106 2000 (Lund et al., 2012). Within the study area, a climate station was established in summer of 1995 and started to  
107 collect the hourly meteorological measurements since then. The local climate type is characterized as “polar desert”  
108 with low precipitation in summer and intensive and persistent coldness for the rest part of the year (Abermann et al.,  
109 2017). Based on the meteorological measurements, annual mean air temperature shows an increase of 0.05 °C yr<sup>-1</sup>  
110 for 1996-2014, and such increased warming is largely attributed to the winter-time warming (i.e. DJF) of 0.15 °C yr<sup>-1</sup>  
111 <sup>1</sup>. Both changes in annual total precipitation and snowfall are less than 1% during 1996-2014. Annual maximum  
112 thawing depth has been observed around 60–70 cm over August and September (Hollesen et al., 2011). *C.*  
113 *tetragona*, an evergreen dwarf shrub species with the average height of 5-10 cm (Elberling et al., 2008; Campioli et  
114 al., 2012) and leaf area index of 0.4-0.5 (Campioli et al., 2009), dominates the surrounding ecosystems by covering  
115 around 53% of surface areas (Bay 1998). Mosses and lichens cover the areas around 8% and 3% respectively. Few  
116 patches of *Salix Arctica*, *Dryas* and other herbs cover less than 5% of the total areas. The surface albedo of summer-  
117 and winter-time varies from 0.15 to 0.8. The soil type is classified as *Typic Psammenturbels*, which locates most soil  
118 C near the surface and a consistently low C concentration for the deeper soil horizons (Elberling et al., 2008). In  
119 some places, the buried organic-rich surface layer at approximately the depth of 20-30 cm was dated to reflect soil  
120 development since the Holocene Climate Optimum around 5000 years ago (Christiansen et al., 2002). Table 1 lists  
121 the information on climate, plant and soil characteristics, some of which are used to set initial conditions of soil and  
122 plant properties in the model and will be mentioned in the following sections.

### 123 2.2 Measurements and data

124 The hourly meteorological data sets for 1996-2014 consist of incoming short-wave and long-wave radiation,  
125 precipitation, 2m air temperature, wind speed, and relative humidity. The daily soil temperatures were measured at  
126 the depth of 0, 60, 130 cm for the same period as the meteorological measurements. Snow depth for 1997-2014 was  
127 measured at every three hours. The CO<sub>2</sub>, sensible heat and latent heat fluxes were measured by the EC technique  
128 based on the half-hour average after being gap-filled or storage-corrected for the period 2000-2014 (Lund et al.,  
129 2012), but they were integrated into the hourly interval for the model comparison. The 2 depths (10 and 30 cm) of  
130 soil water content for 2006-2014 were measured by the Time-Domain Reflectometry (TDR) technique. All these  
131 data sets are available in the Greenland Ecosystem Monitoring database (<http://data.g-e-m.dk/>).

### 132 2.3 Model description

133 The CoupModel (version 5.0, available in <http://www.coupmodel.com>) is a process-oriented ecosystem model with  
134 a number of modules that represent biotic and abiotic processes for heat and mass (i.e. water, C and N) transfer  
135 within an atmosphere-plant-soil continuum and depth-dependent environmental controls on soil C dynamics  
136 (Jansson et al., 2012). The following model description mainly focuses on the processes relevant to this work, and



137 the parameters and equations are provided in the Table S1. A more detailed documentation of principles, parameters  
138 and equations can be found in Jansson and Karlberg (2010).

### 139 **2.3.1 Soil heat and soil water**

140 Soil heat and water flows were estimated using a coupling between the Fourier equations and Richard equations  
141 based on soil physical characteristics of a vertical multi-layered domain (Jansson and Halldin, 1979). In this study,  
142 the soil profile (37.35 m) was prescribed using 35 soil layers with increasing thickness from 0.05m for the top layer  
143 to 3 m for the bottom layer. Soil heat flow only accounted for conduction of heat using the thermal conductivity  
144 function. Soil thermal conductivity was estimated by considering soil texture characteristics, organic matter  
145 thickness, soil water content, and ice content (Kersten, 1949). The upper boundary conditions for soil heat transfer  
146 were regulated by soil surface heat flow, which was calculated using a function of soil surface temperature, organic  
147 layer thickness and convective heat flow given by infiltrated water and vapour. The soil surface temperature was a  
148 weighted sum of the estimation on three conditions: the bare soil, the soil partially covered by snow and the soil  
149 partially covered by plants. This allows soil surface temperature to reflect either the interactions between  
150 aerodynamic properties (e.g. plant cover and bare soil) or the steady-state heat transfer between soil and a  
151 homogeneous snow pack. The lower boundary condition for heat conduction was estimated by a parameter which  
152 represents a constant geothermal heat flow.

153 Soil water was balanced by water infiltrated into the soil, soil evaporation, plant water uptake and runoff. Water  
154 flows between adjacent soil layers were assumed to be laminar, consisting of a matrix flow, a vapour flow and a  
155 macro-pores bypass flow. The upper boundary condition for calculating water flows was given by separate sub-  
156 routines accounting for surface hydrology, soil frost, snow dynamics, and canopies interception of precipitation. The  
157 lower boundary condition of sub-surface hydrology depended on the groundwater level or saturation conditions. The  
158 initial conditions of soil water storage were prescribed by setting soil water content. The drainage and deep  
159 percolation were calculated based on an empirical linear equation.

### 160 **2.3.2 Snow dynamics**

161 The snow pack is an important factor to influence the upper boundary condition of soil heat and water flows and has  
162 been assumed homogeneous both horizontally and vertically in the model. Precipitation was distinguished between  
163 rainfall and snowfall using the temperature as a threshold parameter. Snowmelt was controlled by global radiation,  
164 air temperature and heat flux from the soil. The melting caused by global radiation was to some extent dependent on  
165 snow age. Liquid water retained in the snow pack was allowed to refreeze. The thermal conductivity of snow was  
166 estimated according to snow density. In this study, we used the energy balance approach to calculate snow surface  
167 temperature and sensible and latent heat fluxes upon snow surface (Gustafsson et al., 2004).

### 168 **2.3.3 Plant growth**

169 The potential rate of leaf assimilation was estimated using the light-use efficiency approach, which assumes that the  
170 total plant growth is proportional to the absorbed global radiation but limited by unfavourable conditions of



171 temperature, water and nitrogen (Monteith 1972; Monteith and Moss, 1977). Too high or too low leaf temperatures,  
172 too high leaf C:N ratio and water stress (i.e. the ratio of transpiration to potential transpiration) could stunt plants'  
173 growth and development. The growth stage of plants (e.g. start of growth, leafing and grain development etc.) was  
174 determined according to species types and regulated by temperature sums. The allocation of C to different storage  
175 compartments (root, stem and leaf) was estimated by the multiplicative response of biomass, the leaf C:N ratio and  
176 water stress. The new (the current year) and old (the previous years) C storage compartments were distinguished and  
177 had different rates of litterfall. Plant respiration accounting for both maintenance and growth was simulated using  
178 the exponential “ $Q_{10}$  type” temperature response function (Hansen and Jensen, 1977). The model represented  
179 vegetation structure using the “multiple canopies” approach, which differentiates structure of each canopy stand in  
180 their competence of using the common resources, e.g. light, water and nutrients, for their growth. In our case, we  
181 parameterized two sets of canopy properties corresponding to the dwarf evergreen shrub (i.e. *C. tetragona*) and the  
182 prostrate forbs (i.e. mosses and lichen) respectively. These two canopies had different sizes in surface cover (*C.*  
183 *tetragona*: 53%, mosses: 8%), maximum canopy height (*C. tetragona*: 15 cm, mosses: 5 cm), maximum leaf area  
184 index (*C. tetragona*: 1, mosses: 0.5) and root lowest depth (*C. tetragona*: 20 cm, mosses: 5 cm). The maximum  
185 lifetime of leaves for *C. tetragona* and mosses were set to 3 years and 1 year respectively.

#### 186 **2.3.4 Soil decomposition**

187 At each soil layer, soil organic matter was stored by a litter pool and a humus pool, which had a high and low C  
188 turnover rate correspondingly. The decomposition in both C pools was calculated by following the first order  
189 kinetics and constrained by soil temperature and soil moisture response function. The soil temperature response  
190 function used “Ratkowsky function”, a quadratic function to account for temperature dependency of microbial  
191 activities (e.g. bacterial growth) and was controlled by high and low temperature threshold parameters (Ratkowsky,  
192 1982). The soil moisture response function relied on the parameters which control the dependency curve within the  
193 high and low interval of soil water content (Skopp et al., 1990). Between these two water content intervals, there is  
194 no soil moisture limitation. Since the microbes were implicitly included in the litter pool, the synthesis of microbial  
195 biomass and metabolites constituted internal cycling. The initial values for the C and N content in each soil layer  
196 were prescribed by measurements and partitioned into the two pools for each layer according to the measured C:N  
197 ratio and soil bulk density as described in Table 1.

#### 198 **2.4 Model setup, calibration and evaluation**

199 The model used the hourly meteorological measurements (i.e. 2m air temperature, precipitation incoming shortwave  
200 and longwave radiation, wind speed, and relative humidity) as drivers. By assuming vegetation started to grow from  
201 an equilibrium state, we implemented a 90-year run which was repeatedly driven by the meteorological  
202 measurements of 1996 as a model spin-up. We applied the GLUE (Generalized Likelihood Uncertainty Estimation,  
203 Jansson, 2012) framework to calibrate the model. The GLUE framework adopts a Monte-Carlo based approach to  
204 reduce parameter uncertainties of the prior runs and thus attain the behaviour model ensembles of accepted runs. It  
205 normally involves the following procedures: (I) to define the acceptance criteria; (II) to select uncertain parameters;



206 (III) to assign range and distribution functions for selected parameters; (IV) random realization of the model with  
207 independence between parameters and previous runs (Wetterstedt & Ågren, 2011).

208 In this study, we performed a 19,000 Monte-Carlo multi-run based on the stochastic sampling of 33 parameters  
209 (Table 2). The minimum and maximum values of the sampled parameters were given in the Table 2. We used  
210 performance indexes (i.e. mean errors - ME and root mean square errors – RMSE) to select around 30 posterior runs  
211 based on the calibration against the time-integrated CO<sub>2</sub> fluxes (Table 3). It is noted that the acceptance criteria is  
212 subjective and attained after we have conducted several initial selection tests. The time-integrated CO<sub>2</sub> fluxes refer  
213 to the hourly measurements of NEE being transformed to cumulative sequences of fluxes for a day, a year and the  
214 entire measurement period. The NEE measurements were not gap-filled. Therefore, the transformations were made  
215 to smooth out uncertainties in single measured point and rather emphasize the pattern of flux within the day, within  
216 the year or for the long-term trend of the measurements. We calibrated the model based on the transformed NEE  
217 fluxes. After calibration, the corresponding behaviour model ensembles were named “the diurnal behaviour model  
218 ensemble (DBME), the seasonal behaviour model ensemble (SBME) and the long-term behaviour model ensemble  
219 (LBME)”.

220 To identify the importance of controlling parameters and relevant processes reflected by the three behaviour model  
221 ensembles, we calculated the *Pearson* correlation between posterior parameters and R<sup>2</sup> (the coefficient of  
222 determination for linear regression) of each measurement variable, and the inter-correlation matrix of parameters.  
223 We use the mean, coefficient of variation (CV, the standard deviation divided by the mean), skewness and kurtosis  
224 of probability density function (PDF) and cumulative distribution of frequency (CDF) to describe how well the  
225 posterior parameters have been constrained by each behaviour model ensemble. Finally, the mean and trend for the  
226 inter-annual variation of internal C fluxes and C storage pools in the three behaviour model ensembles were  
227 presented.

## 228 **2.5 Spectral analysis**

229 In order to investigate how well the three behaviour model ensembles were constrained to reflect multiple time  
230 scales of ecosystem behaviours, we calculated a multiscale variance of “maximal overlap discrete wavelet  
231 transform” (MODWT) for the measured and simulated CO<sub>2</sub> fluxes. This approach decomposes the data sets into  
232 time-varying components to reveal the data patterns within single time window. The wavelet analysis was conducted  
233 using the Matlab wavelet toolbox on the basis of the “Haar” mother wavelet, which has been widely used to analyse  
234 the atmospheric turbulence data (Hudgins et al., 1993). We firstly pre-processed the data sets by replacing all the  
235 missing values in the measurements with 0 so as to have a complete time series. The model results only selected the  
236 values within the measurement dates and used 0 for the days with no measurements. The wavelet decomposition  
237 was performed for 15 levels. Each level corresponds to different time window length with the power of 2 at hours.



## 238 3 Results

### 239 3.1 Wavelet detection of time-varying variance for the measurements and model ensemble means

240 The variance of MODWT for the measured and modelled CO<sub>2</sub> fluxes was presented over the time scales in power of  
241 2 for hours based on 15 transformed levels (Fig. 2). Accordingly, the patterns of the variance changing from the  
242 diurnal scale (hours) to the inter-annual scale (a year, equivalent to 2<sup>13.09</sup> hours) were well distinguished for each  
243 time series of dataset. The behaviour model ensemble means generally agreed well with the measurements in the  
244 patterns of variance across a wide range of time scales, but differed a bit in the magnitude at some individual time  
245 windows. Within the daily to weekly time scale (i.e. from 2<sup>2</sup> to 2<sup>7</sup> hours), DBME showed fewer deviations from the  
246 measurements than the other two model ensembles, and LBME showed the largest deviation from the  
247 measurements. On the contrary, at a relatively long time scale (e.g. 2<sup>9</sup> to 2<sup>11</sup> hours), the least deviation between the  
248 measurements and the model was found in LBME.

### 249 3.2 Evaluation of the behaviour model performance

#### 250 3.2.1 The model performance in simulating the measurement variables

251 The posterior runs effectively constrained the prior NEE fluxes by narrowing down the range of ME and RMSE  
252 (Fig. 3). All the behaviour model ensembles displayed a symmetrical Gaussian distribution of ME in NEE centring  
253 on 0 (Fig. 3a). They also showed their capabilities to best describe the time-scale integrated C fluxes based on their  
254 defined behaviours (Fig. 3b-3c). For instance, the smallest RMSE for the daily-integrated NEE was found in DBME  
255 (Fig. 3b), and this is similar to SBME and LBME, which had the smallest RMSE in the yearly-integrated NEE and  
256 the entire period-integrated NEE respectively (Fig. 3c and 3d). Despite that the model used the observed NEE as the  
257 only constraint, the other measurement variables were fairly well simulated (Fig. 4). It implies the holistic ecosystem  
258 dynamics represented by the model is reasonably consistent. In each ensemble, R<sup>2</sup> of most measurement variables  
259 was larger than 0.5 and the averaged ME was close to 0. However, the model showed a relatively large  
260 underestimation on soil water content (SW<sub>0.1m</sub> and SW<sub>0.3m</sub>) and latent heat flux (LHF) (Fig. 4a). The relatively low  
261 R<sup>2</sup> in NEE in DBME was partly due to the large uncertainties in simulating the autumn-time NEE (NEE<sub>Oct</sub>), which  
262 had a lower R<sup>2</sup> than NEE and NEE of growing season (NEE<sub>Jul-Oct</sub>). It is noted that R<sup>2</sup> of the calibrated variables is  
263 sensitive to the length of a cumulative time sequence so that R<sup>2</sup> became larger as the cumulative time sequence was  
264 lengthened. Although all the ensembles had overestimated snow depth, they still simulated reasonable soil  
265 temperatures by using the posterior parameters.

#### 266 3.2.2 The model residuals allocated at the diurnal, seasonal and long-term time scales

267 The residuals between the model and measurements were allocated for the diurnal, seasonal and long-term course  
268 (Fig. 5). The diurnal patterns of the hourly-mean residuals showed that the model overestimated C uptake during the  
269 daytime and C release during the night-time. LBME showed a wider uncertainty band and greater amplitude of the  
270 residuals than the other two ensembles (Fig. 5a). For the seasonal patterns of the daily mean residuals, the model  
271 overestimated C uptake in early spring and later autumn and C release in summer, and DBME and SBME had a



272 lower amplitude of deviations than LBME (Fig. 5b). In autumn, SBME showed fewer residuals than DBME. For the  
273 total cumulative residuals, LBME was constrained much better than the other two ensembles (Fig. 5c). In particular,  
274 DBME seemed to have divergent trends for the inter-annual variation of the cumulative residuals. For the period  
275 2000-2007, a positive bias was propagated, but for the period 2008-2014, a negative bias tended to offset the  
276 positive bias and resulted in a good balance of the two at the end of the period.

### 277 3.3 Assessment of the ecosystem C budget and trends

#### 278 3.3.1 Inter-annual and seasonal variation of NEE

279 All the model ensembles showed a similar inter-annual and seasonal variation of NEE, but they also differed in the  
280 slope of the linear trend and the year-round C budget (Fig. 6). The annual mean NEE started from a positive value  
281 (C source) at 2000 and varied towards a negative value (C sink) in most years (Fig. 6a). All of the ensembles  
282 reached the highest C uptake in 2008. After 2008, there was no trend for DBME, but both SBME and LBME  
283 indicated that the annual NEE tended to shift towards a C source. However, for the entire period, only DBME  
284 showed a significant downward trend of NEE (Table 4). For the seasonal profile of NEE, the NEE started from a C  
285 source in early spring and became an increased C sink in the growing season, and then was offset by increased C  
286 release in autumn (Fig. 6b). DBME showed the highest C uptake in summer and the lowest C release in spring and  
287 autumn. The year-round C budget for the three ensembles showed the ecosystem approximated to either a week sink  
288 (i.e. DBME:  $-9.8 \pm 4.4 \text{ g C m}^{-2} \text{ yr}^{-1}$  and SBME:  $-4.1 \pm 4.7 \text{ g C m}^{-2} \text{ yr}^{-1}$ ) or a neutral C balance (LBME:  $-0.1 \pm 6.4 \text{ g C}$   
289  $\text{m}^{-2} \text{ yr}^{-1}$ ).

#### 290 3.3.2 The mean C budget and the temporal trends for C fluxes and stores based on the behaviour model 291 ensemble mean

292 In general, compared to the long-term behaviour model ensemble, the short-term behaviour model ensemble showed  
293 a lower estimate for the mean C flux rates and the plant-associated C storage pools and a higher estimate for the soil  
294 C pools (Table 4). All the three behaviour model ensembles displayed a slightly increasing trend for the ecosystem C  
295 uptake (i.e. the negative NEE trend), but only the trend of DBME was significant (Table 4). Other significant trends  
296 in DBME were found in the inter-annual variation of GPP, ER, plant respiration ( $R_{\text{plant}}$ ), root respiration ( $R_{\text{root}}$ ),  
297 litterfall, and all the C pools but the litter pool ( $C_{\text{litter}}$ ). By contrast, LBME had the fewest number of C fluxes with  
298 significant trends. The GPP and ER simulated by DBME were  $-59.4 \pm 16.1 \text{ g C m}^{-2} \text{ yr}^{-1}$  and  $41.3 \pm 4.4 \text{ g C m}^{-2} \text{ yr}^{-1}$   
299 respectively, around 60% of the C flux rates estimated by LBME. The difference of C balance in the three model  
300 ensembles was largely subject to the proportion of soil  $\text{CO}_2$  production. The fractions of respiration for humus and  
301 soil (i.e.  $R_{\text{humus}}$  and  $R_{\text{soil}}$ ) in DBME, SBME and LBME were 20.8%, 27.8% and 33.3% respectively. A higher portion  
302 of soil respiration simulated by LBME originated from changes in the soil humus pool ( $C_{\text{humus}}$ ), indicating a larger  
303 amount of old C release. Opposed to the trend of  $C_{\text{litter}}$ , the trend of  $C_{\text{humus}}$  was found significant for all the  
304 ensembles, with a higher magnitude for a longer term behaviour model ensemble. It is noted that the moss C pool  
305 ( $C_{\text{moss}}$ ) was higher in DBME than that in SBME and LBME.



### 306 3.4 Sensitivities and uncertainties of posterior parameters

#### 307 3.4.1 Sensitivities of posterior parameters to model performance

308 We counted the number of posterior parameters with the *Pearson* correlation coefficient for linear regression ( $r >$   
309  $0.3$  or  $r < -0.3$ ) to the posterior  $R^2$  of the measurement variables and grouped them into the processes they belonged  
310 to. This helped us to identify which processes were important to which measurement variables and how this  
311 indication differed among the model ensembles. All the model ensembles showed a certain pattern on the count of  
312 sensitive parameters for their posterior values and  $R^2$  of the measurement variables (Fig. 7). The parameters were  
313 grouped into the processes of snow dynamics, soil water and soil heat, plant growth, and soil decomposition. The  
314 surface temperature ( $ST_{0m}$ ) was highly associated with the parameters in the processes of snow dynamics, soil heat  
315 and soil water and plant growth. But for soil temperature at the depth of 0.6 m and 1.3 m (i.e.  $ST_{0.6m}$  and  $ST_{1.3m}$ ),  
316 LBME showed the sensitive parameters belonged to the processes of soil decomposition. For the soil water content  
317 at 0.1 m ( $SW_{0.1m}$ ), parameters from all the processes were sensitive to the model performance, but this differed from  
318 the soil water content at 0.3 m ( $SW_{0.3m}$ ), which may exclude parameters from one or another process. The sensitive  
319 parameters to snow depth common to all the model ensembles were from the processes of plant growth and snow  
320 dynamics. For the radiation fluxes, the common sensitive parameters were from the processes of plant growth, snow  
321 dynamics and soil water and soil heat. The parameters in the process of soil decomposition appeared sensitive to  
322 latent heat flux in both SBME and LBME. For NEE of the entire period or sub-periods, the soil decomposition  
323 parameters increased their number in the longer time behaviour models. Overall, the performance of SBME for most  
324 measurement variables was correlated to the parameters from all the four processes, while in DBME, more  
325 correlations were found in the parameters associated with snow dynamics and soil water and heat transfer, and in  
326 LBME, more correlations were found in the parameters associated with soil decomposition. Most parameters  
327 associated with plant growth showed higher sensitivities than other parameters in all the three model ensembles.

#### 328 3.4.2 Inter-correlations between posterior parameters

329 The inter-correlations between posterior parameters reflected how close the inter-links of processes were controlled  
330 by the parameters in the behaviour models. This may infer that the data used to constrain the model was not suitable  
331 to distinguish various possible explanation to the measurements or that the ecosystem had an inherent dependence  
332 between different properties. The *Pearson* correlation coefficient for linear regression ( $r > 0.3$  or  $r < -0.3$ ) was  
333 adopted to indicate a moderate or high correlation between parameters. Among all the model ensembles, DBME  
334 showed that parameters with a higher number of significant correlations to others were from the processes of snow  
335 dynamics; plant respiration and soil decomposition (Fig. S3a, e.g. *DensityCoefWater* (4), *AlbSnowMin* (4),  
336 *EquiAdjustPsi* (4), *RootRate* (4), *RateCoefLitter* (4), *RateCoefHumus* (5), *TempMin* (6); it is noted that the number  
337 within the brackets indicates the number of parameters with a significant correlation). SBME showed that  
338 parameters with a higher number of significant correlations to others were relevant to snow density, surface  
339 evaporation, surface temperature, and plant growth (Fig. S3b, e.g. *DensityOfNewSnow* (4), *EquiAdjustPsi* (5),  
340 *CFrozenSurfCorr* (5), *TLMIn* (4), *rOptimum\_value* (6), *FixNsupply* (6), *MCoefLeaf* (5)). LBME revealed more  
341 number of significant inter-correlations for parameters were related to the processes of soil heat and water and plant



342 growth (Fig. S3c, e.g. *RoughLMomSnow* (5), *DensityCoefMass* (5), *EquiAdjustPsi* (4), *FreezepointFWi* (6), *TLMIn*  
343 (7), *TLOpt1*(5), *TempMin* (5)). In general, we conclude that DBME showed more unconstrained parameters in soil  
344 decomposition, which however showed the best constraint in LBME. SBME revealed more inter-correlation for  
345 parameters in plant growth, indicating that more equifinalities may exist in this posterior ensemble.

### 346 3.4.3 Posterior distribution of calibrated parameters

347 Most parameters showed a negative kurtosis indicating that the posterior PDF of parameters had a larger combined  
348 weight of the tails relative to the rest of the distribution, and thus their distribution had a flatter peakedness  
349 comparing to the normal distribution (Table 2). Few parameters (e.g. *RoughMomSnow* in DBME and LBME,  
350 *EquiAdjustPsi* in DBME, *TLOpt1* in LBME, *TLMMax* in SBME and *RateCoefHumus* in DBME) showed a relatively  
351 high skewed distribution (i.e. skewness is  $<-1$  or  $>1$ ). In the process of snow dynamics, *RoughLMomSnow* and  
352 *AlbSnowMin* were better constrained than other parameters (Fig. 8). In the process of soil heat and water transfer, all  
353 the model ensembles provided a similar posterior PDF for the parameter *OrganicLayerThick* and larger differences  
354 for the parameters *EquiAdjustPsi*, *CFrozenSurfCorr*, *SurfCoef* and *FreezepointFWi*. In the process of plant growth,  
355 a better constraint on the posterior PDF in the model ensembles was found on the parameters related to the  
356 temperature response function of photosynthesis (i.e. *TLMIn*, *TLOpt1*, *TLOpt2* and *TLMMax*) and plant respiration  
357 (*MCoefLeaf*, *MCoefRoot*, *ResptemQ10* and *rOptimum*). The parameters governing the litterfall rates of leaf and root  
358 (i.e. *LeafRate* and *RootRate*) showed a similar constraint in all the three model ensembles. In the process of soil  
359 decomposition, the model ensembles displayed distinguished patterns for all the parameters, for instance, the rate  
360 coefficient of humus (*RateCoefHumus*) suggested much lower and higher posterior means by DBME and LBME  
361 respectively.

## 362 4. Discussions

### 363 4.1 Model performance and parameter uncertainties

364 Our model ensembles demonstrate the strength of describing the variability of C fluxes at diurnal, seasonal and  
365 long-term time scales. The wavelet analysis further supports that the model constrained using the time-integrated  
366 CO<sub>2</sub> flux has effectively distinguished the model behaviour by matching the observational variance across discrete  
367 time windows. The multi-yearly mean of NEE for 2000-2014 represented by the model ensemble means ranges from  
368  $-9.8 \pm 10.4$  g C m<sup>-2</sup> of DBME to  $-0.1 \pm 10.5$  g C m<sup>-2</sup> yr<sup>-1</sup> of LBME, which are higher than the growing season NEE  
369 measurements reported by previous studies for the same site (e.g.  $-12.4 \pm 8.7$  g C m<sup>-2</sup> yr<sup>-1</sup> for the period of 1997 and  
370 2000-2003 by Grøndahl et al. (2007) and  $-20.6 \pm 11$  g C m<sup>-2</sup> yr<sup>-1</sup> for 2000-2014 by Lund et al. (2012)). The large  
371 year-to-year variability of NEE cannot distinguish the ecosystem as a significant C sink or source, and the  
372 uncertainties of ensemble runs can even further enlarge the year-to-year variability of NEE. Many other modelling  
373 studies (e.g. McGuire et al. (2012); Fisher et al. (2014); Zhang et al. (2013a)) also showed that the process-based  
374 models have simulated the present-day tundra as a weak C sink, but most of these models have only been calibrated  
375 by the growing season NEE measurements. Lund et al. (2012) used a light response curve model to estimate GPP by



376 subtracting the daytime respiration. Their growing season GPP and ER for 2000-2010 were  $-78.6 \pm 13.7 \text{ g C m}^{-2} \text{ yr}^{-1}$   
377 and  $-57.9 \pm 11.4 \text{ g C m}^{-2} \text{ yr}^{-1}$  respectively. In contrast, this study is based on a process-oriented model to estimate the  
378 yearly budget of NEE. For other sites in pan-Arctic, the year-round measurements in Svalbard and Alaska all  
379 indicate that the current tundra ecosystem is now in the transition from a C sink to a C source (e.g. Oechel et al.,  
380 2014; Lüers et al., 2014 and Euskirchen et al., 2016). Particularly, Euskirchen et al. (2016) reported a *C. tetragona*  
381 heath ecosystem in the Alaskan Arctic tundra had a yearly NEE around  $20 \text{ g C m}^{-2}$  for 2014-2015, which was largely  
382 affected by the freezing time of active layers. In our study, LBME showed a larger tendency for ecosystems to  
383 become a C source by suggesting a higher amplitude for the diurnal  $\text{CO}_2$  flux and a higher rate of humus  
384 decomposition. This implies that a faster C cycling, a higher rate of  $\text{CO}_2$  release associated with the old C  
385 decomposition rate and the thawing depth can be possible drivers for the ecosystem sink-source transition.

386 The model-measurement residuals appearing at the same time scale across all the model ensembles imply that the  
387 model may need more measurement variables as additional constraints or examine the model structure or  
388 parameterization. For instance, to address the bias in the diurnal cycle, the sub-daily soil temperatures should be  
389 included in the calibration. For the diurnal NEE, we found a negative bias occurred at noon and a positive bias  
390 occurred in the evening. Both biases are likely associated with the absorbed light in the early spring and mid-  
391 summer (Fig. S1). In the model, the simulated leaf area and snow coverage are important factors to estimate the  
392 absorbed light correctly. In the seasonal cycle, the negative bias in the early growing seasons can be attributed to the  
393 earlier photosynthesis occurring in the model (Fig. S2). Some studies (e.g. Mäkelä et al., 2004; Mellander et al.,  
394 2008; Wu et al., 2012b) showed that boreal ecosystems may encounter the effects of thermal acclimation for  
395 photosynthesis in the early spring, which can delay the start of the photosynthesis. Soil moistures should be an  
396 additional constrain for the growing season GPP and ER, because the freezing and thawing of active layers is highly  
397 dependent on the soil moisture. To address the bias of NEE occurring in the long-term time scale, the biophysical  
398 properties of plants should be included as the model calibration variables or the model drivers.

399 The behaviour model ensembles showed different emphasis on the specific processes which affect the performance  
400 of the model to simulate measurement variables, but the plant growth processes were the common processes having  
401 more sensitive parameters than other processes in all the ensemble runs. The posterior uncertainties of many  
402 parameters were substantially reduced, and some of them show the distinguished patterns in the three model  
403 ensembles. The exponential coefficient in the  $Q_{10}$  equation for plant respiration were suggested a higher value range  
404 (2.75-3.5) than the default value (0.5 -1.75). The default value was often applied to the boreal forests, which had  
405 warmer ambient temperature. Higher  $Q_{10}$  indicates the temperature sensitivities is lower in the lower temperature but  
406 higher in the warm temperature (i.e.  $20^\circ\text{C}$ ) in our study. All the model ensembles suggested a lower temperature as  
407 the cold threshold for temperature response of soil respiration, indicating a convergence of temperature sensitivity.  
408 Further, there may have some equifinalities for the posterior parameters, which allow different parameter sets to  
409 provide equal efficiency to describe the system, and suggest right estimates because of wrong reasons. This issue  
410 can be addressed by adding more independent data to constrain the model (William et al., 2009; Carvalhais et al.,  
411 2010).



412 **4.2 Important drivers for the diurnal, seasonal and long-term behaviours of ecosystem CO<sub>2</sub> exchange in high**  
413 **Arctic tundra**

414 To elucidate important drivers for the temporal behaviours of ecosystem CO<sub>2</sub> exchange, we presented the diagnostic  
415 variables (i.e. the response anomaly) to indicate how photosynthesis and ER are regulated by their responses to air  
416 temperature and water stress, absorbed radiation and responses of litter and humus decomposition varying at the  
417 daily, seasonal and long-term time scales. The responses of litter and humus decomposition have accounted for  
418 depth-specific soil temperature, soil moisture and substrate concentration. The largest diurnal deviation in the  
419 absorbed radiation was found highest at noon but lowest at night (Fig. 9). The temperature response showed positive  
420 anomaly in the daytime with a larger portion in the afternoon. The response of humus and litter respiration occurred  
421 mostly in the afternoon, whereas soil moisture response was much lower in the daytime than night-time. For the  
422 seasonal profile, the highest temperature response occurred in the mid-growing season, and the absorbed radiation  
423 started earlier in conjunction with the snowmelt period. The humus and litter respiration also had a higher responses  
424 in the mid-summer but humus respiration response seemed to have a little delayed than litter response, possibly  
425 because of the delayed response of deeper soil horizons where old carbon has a larger proportion. The soil moisture  
426 response decreased in the growing season, and a larger decrease was seen in autumn. For the long-term scale, the  
427 response of litter respiration and soil moisture seem to level off for the entire period, while the humus respiration  
428 response had a little reduction in the last few years. The year-to-year variation of litter and humus respiration  
429 response is largely in line with the tendency of temperature response. The absorbed radiation and temperature  
430 response showed a large increase before 2008 and level off for the rest the period. The absorbed radiation to some  
431 extent reflected the biological properties response. For instance, the surface albedo has a high decrease in the first  
432 half period than the second half period because of changes in vegetation cover. Note that all the above-mentioned  
433 responses were quantified by the corresponding time scale behaviour model ensemble means.

434 **4.3 Implication for both modelling and measurements**

435 Our study demonstrates a clear trade-off when the model is tuned to capture both the short- and long-term patterns in  
436 ecosystem CO<sub>2</sub> exchange. This agrees the previous findings that environmental and biotic factors might represent  
437 different roles in explaining fluctuations in CO<sub>2</sub> fluxes across time scales (Richardson et al. 2007; Wu et al., 2012a;  
438 Wu et al., 2017). However, as we have not validated the model with any observation that reflects seasonal and inter-  
439 annual variabilities of biological responses, for instance, canopy cover or LAI, we cannot conclude that the large  
440 bias in the total cumulative CO<sub>2</sub> fluxes in DBME is attributed to uncertainties in model parameterization or model  
441 structure deficiency. The former uncertainties can be addressed by using observations to prescribe the dynamics of  
442 parameters, (e.g. LAI). The latter uncertainties can be addressed by including processes which describe a more  
443 appropriate seasonal pattern of ecosystem dynamics. For instance, the overestimated C uptake appeared frequently  
444 in spring for several years. This implies that the model may have to account for thermal acclimation effects of  
445 photosynthesis to explain the delay of C uptake. LBME suggests a more precise description of long-term behavior of  
446 CO<sub>2</sub> fluxes by estimating a faster turnover rate of soil C pool. This also highlights that to quantify the turnover rate  
447 of soil C is crucial to project the long-term trend of ecosystem CO<sub>2</sub> exchange.



448 The high frequency of measurements used in this study allows the process-oriented model to identify the main  
449 drivers for variation of C fluxes across the wide range of time scales and to quantify the year-around C budget. The  
450 process-oriented modelling with a strong emphasis on the balance of energy, water and carbon at a high resolution  
451 for soil profile and temporal evolution has demonstrated the efficiency in process representation and the challenges  
452 of capturing both short-term and long-term CO<sub>2</sub> variation. The non-growing season respiration and the burst events  
453 of CO<sub>2</sub> efflux in spring in relation to seasonal and future climate trends calls for the extension of monitoring  
454 campaign to cover the entire non-growing-seasons. Moreover, it is important to investigate to which extent the early  
455 spring burst originates from the winter CO<sub>2</sub> production and the partition of soil CO<sub>2</sub> production from the  
456 decomposition of labile C storage and old C storage located at the near-surface horizon. To compromise the  
457 uncertainties of winter precipitation, snow properties like snow cover extent and snow water equivalent are of high  
458 interest in that they determine soil temperature and moisture conditions for the non-growing season respiration to  
459 regulate the current transition of NEE. Further studies are needed to investigate plant growth (i.e. photosynthesis and  
460 respiration) in the subnivean microclimate.

## 461 5. Conclusions

462 This study demonstrates that three behaviour model ensembles constrained by the time-integrated CO<sub>2</sub> fluxes using  
463 the Monte-Carlo runs were able to describe the variation of 15 years of eddy covariance NEE measurements for a  
464 high Arctic heath ecosystem on a daily, seasonal and long-term basis. The inter-annual variation of NEE showed a  
465 trend from the ecosystem being a C sink to a C neutral balance for all the three behaviour model ensembles. The  
466 long-term behaviour model ensemble simulated a more intensified diurnal C cycle than the short-term behaviour  
467 model ensemble. The intensified C cycle was mainly attributed to a faster depletion of soil C pools and higher  
468 amplitude of diurnal CO<sub>2</sub> variation. The correlations of posterior parameters and R<sup>2</sup> reflected that parameters in the  
469 processes of soil water and heat and snow dynamic regulated the short-term behaviour of CO<sub>2</sub> fluxes, while  
470 parameters in soil decomposition processes regulated the long-term behaviour of CO<sub>2</sub> fluxes. Our results suggest  
471 that using the time-integrated CO<sub>2</sub> fluxes as model constraints can be a good diagnostic approach to evaluate how  
472 the performance of the model is appropriate for different time scales of processes and if there is any transition in  
473 ecosystem processes the model misrepresents. However, more efforts in quantifying models' uncertainties and more  
474 independent measurements are still needed to further improve our understanding the key drivers of high Arctic  
475 ecosystems C dynamics associated with substantial changes observed in the environmental conditions.

## 476 Acknowledgements

477 This work was supported by a grant from the Danish National Research Foundation (CENPERM DNRF100). We  
478 are grateful to Greenland Ecosystem Monitoring program for kindly providing all of data for this study. The  
479 software "CoupModel" is freely downloadable through the webpage (<http://www.coupmodel.com>). The source code  
480 can be requested for non-commercial purposes from Per-Erik Janson ([pej@kth.se](mailto:pej@kth.se)). Meteorological data and C flux  
481 data are available from Greenland Ecosystem Monitoring Database (<http://data.g-e-m.dk/>).



482 **References**

- 483 AMAP: Snow, Water, Ice and Permafrost in the Arctic (SWIPA): Climate Change and the Cryosphere, Arctic  
484 Monitoring and Assessment Programme (AMAP), Oslo, Norway, xii + 538 pp., 2011.
- 485 Abermann, J., Hansen, B., Lund, M., Wacker, S., Karami, M., and Cappelen, J.: Hotspots and key periods of  
486 Greenland climate change during the past six decades, *AMBIO*, 46, 3-11, 10.1007/s13280-016-0861-y, 2017.
- 487 Arndal, M. F., Illeris, L., Michelsen, A., Albert, K., Tamstorf, M., and Hansen, B. U.: Seasonal variation in gross  
488 ecosystem production, plant biomass, and carbon and nitrogen pools in five high Arctic vegetation types, Arctic,  
489 Antarctic, and Alpine Research, 41, 164-173, 2009.
- 490 Baldocchi, D., Falge, E., and Wilson, K.: A spectral analysis of biosphere–atmosphere trace gas flux densities and  
491 meteorological variables across hour to multi-year time scales, *Agric. For. Meteorol.*, 107, 1-27, 2001.
- 492 Baldocchi, D., Chu, H., and Reichstein, M.: Inter-annual variability of net and gross ecosystem carbon fluxes: A  
493 review, *Agric. For. Meteorol.*, 10.1016/j.agrformet.2017.05.015, 2017.
- 494 Bay, C.: Vegetation mapping of Zackenberg valley, Northeast Greenland. København, 75pp, 1998.
- 495 Blok, D., Weijers, S., Welker, J. M., Cooper, E. J., Michelsen, A., Löffler, J., and Elberling, B.: Deepened winter  
496 snow increases stem growth and alters stem  $\delta^{13}\text{C}$  and  $\delta^{15}\text{N}$  in evergreen dwarf shrub *Cassiope tetragona* in high-  
497 Arctic Svalbard tundra, *Environ. Res. Lett.*, 10, 044008, 2015.
- 498 Blok, D., Elberling, B., and Michelsen, A.: Initial stages of tundra shrub litter decomposition may be accelerated by  
499 deeper winter snow but slowed down by spring warming, *Ecosystems*, 19, 155-169, 2016.
- 500 Braswell, B. H., Sacks, W. J., Linder, E., and Schimel, D. S.: Estimating diurnal to annual ecosystem parameters by  
501 synthesis of a carbon flux model with eddy covariance net ecosystem exchange observations, *Glob. Chang. Biol.*,  
502 11, 335-355, 2005.
- 503 Campioli, M., Street, L. E., Michelsen, A., Shaver, G. R., Maere, T., Samson, R., and Lemeur, R.: Determination of  
504 Leaf Area Index, Total Foliar N, and Normalized Difference Vegetation Index for Arctic Ecosystems Dominated by  
505 *Cassiope tetragona*, *Arct., Antarc., Alp. Res.*, 2009.
- 506 Campioli, M., Leblans, N., and Michelsen, A.: Stem Secondary Growth of Tundra Shrubs: Impact of Environmental  
507 Factors and Relationships with Apical Growth, *Arct., Antarc., Alp. Res.*, 2012.
- 508 Carvalhais, N., Reichstein, M., Ciais, P., Collatz, G. J., Mahecha, M. D., Montagnani, L., Papale, D., Rambal, S.,  
509 and Seixas, J.: Identification of vegetation and soil carbon pools out of equilibrium in a process model via eddy  
510 covariance and biometric constraints, *Glob. Change Biol.*, 16, 2813–2829, 2010.
- 511 Christiansen, H. H., Bennike, O., Böcher, J., Elberling, B., Humlum, O., and Jakobsen, B. H.: Holocene  
512 environmental reconstruction from deltaic deposits in northeast Greenland, *J. Quat. Sci.*, 17, 145-160, 2002.
- 513 Dietze, M. C., Vargas, R., Richardson, A. D., Stoy, P. C., Barr, A. G., Anderson, R. S., Arain, M. A., Baker, I. T.,  
514 Black, T. A., Chen, J. M., Ciais, P., Flanagan, L. B., Gough, C. M., Grant, R. F., Hollinger, D., Izaurrealde, R. C.,



- 515 Kucharik, C. J., Lafleur, P., Liu, S., Lokupitiya, E., Luo, Y., Munger, J. W., Peng, C., Poulter, B., Price, D. T.,  
516 Ricciuto, D. M., Riley, W. J., Sahoo, A. K., Schaefer, K., Suyker, A. E., Tian, H., Tonitto, C., Verbeeck, H., Verma,  
517 S. B., Wang, W., and Weng, E.: Characterizing the performance of ecosystem models across time scales: A spectral  
518 analysis of the North American Carbon Program site-level synthesis, *Journal of Geophysical Research:*  
519 *Biogeosciences*, 116, G04029, 2011.
- 520 Elberling, B.: Seasonal trends of soil CO<sub>2</sub> dynamics in a soil subject to freezing, *Journal of Hydrology*, 276, 159-  
521 175, 2003.
- 522 Elberling, B., Jakobsen, B. H., Berg, P., Søndergaard, J., and Sigsgaard, C.: Influence of vegetation, temperature,  
523 and water content on soil carbon distribution and mineralization in four high Arctic soils, *Arctic, Antarctic, and*  
524 *Alpine Research*, 36, 528-538, 2004.
- 525 Elberling, B., Nordstrøm, C., Grøndahl, L., Søgaard, H., Friborg, T., Christensen, T. R., Ström, L., Marchand, F.,  
526 and Nijs, I.: High-Arctic Soil CO<sub>2</sub> and CH<sub>4</sub> Production Controlled by Temperature, Water, Freezing and Snow, in:  
527 *Advances in Ecological Research*, Academic Press, 441-472, 2008.
- 528 Elberling, B., Michelsen, A., Schadel, C., Schuur, E. A. G., Christiansen, H. H., Berg, L., Tamstorf, M. P., and  
529 Sigsgaard, C.: Long-term CO<sub>2</sub> production following permafrost thaw, *Nat. Clim. Change*, 3, 890-894, 2013.
- 530 Elmendorf, S. C., Henry, G. H. R., Hollister, R. D., Björk, R. G., Bjorkman, A. D., Callaghan, T. V., Collier, L. S.,  
531 Cooper, E. J., Cornelissen, J. H. C., Day, T. A., Fosaa, A. M., Gould, W. A., Grétarsdóttir, J., Harte, J., Hermanutz,  
532 L., Hik, D. S., Hofgaard, A., Jarrad, F., Jónsdóttir, I. S., Keuper, F., Klanderud, K., Klein, J. A., Koh, S., Kudo, G.,  
533 Lang, S. I., Loewen, V., May, J. L., Mercado, J., Michelsen, A., Molau, U., Myers-Smith, I. H., Oberbauer, S. F.,  
534 Pieper, S., Post, E., Rixen, C., Robinson, C. H., Schmidt, N. M., Shaver, G. R., Stenström, A., Tolvanen, A.,  
535 Totland, Ø., Troxler, T., Wahren, C.-H., Webber, P. J., Welker, J. M., and Wookey, P. A.: Global assessment of  
536 experimental climate warming on tundra vegetation: heterogeneity over space and time, *Ecol. Lett.*, 15, 164-175,  
537 2012.
- 538 Groendahl, L., Friborg, T., and Soegaard, H.: Temperature and snow-melt controls on inter-annual variability in  
539 carbon exchange in the high Arctic, *Theor Appl Climatol*, 88, 2007.
- 540 Gaumont-Guay, D., Black, T. A., Barr, A. G., Jassal, R. S., and Nesic, Z.: Biophysical controls on rhizospheric and  
541 heterotrophic components of soil respiration in a boreal black spruce stand, *Tree Physiology*, 28, 161-171, 2008.
- 542 Grosse, G., Scott, G., McGuire, A. D., Vladimir, E. R., and Edward, A. G. S.: Changing permafrost in a warming  
543 world and feedbacks to the Earth system, *Environ. Res. Lett.*, 11, 040201, 2016.
- 544 Gustafsson, D., Waldner, P. A., and Stähli, M.: Factors governing the formation and persistence of layers in a  
545 subalpine snowpack, *Hydrol. Process.*, 18, 1165-1183, 2004.
- 546 Hansen, G. K., and Jensen, C. R.: Growth and Maintenance Respiration in Whole Plants, Tops, and Roots of *Lolium*  
547 *multiflorum*, *Physiol. Plant.*, 39, 155-164, 1977.



- 548 Hollesen, J., Elberling, B., and Jansson, P. E.: Future active layer dynamics and carbon dioxide production from  
549 thawing permafrost layers in Northeast Greenland, *Glob. Chang. Biol.*, 17, 911-926, 2011.
- 550 Hudgins, L., Friehe, C. A., and Mayer, M. E.: Wavelet transforms and atmospheric turbulence. *Phys. Rev. Lett.*, 71,  
551 3279, 1993.
- 552 Hugelius, G., Strauss, J., Zubrzycki, S., Harden, J. W., Schuur, E. A. G., Ping, C. L., Schirmer, L., Grosse, G.,  
553 Michaelson, G. J., Koven, C. D., O'Donnell, J. A., Elberling, B., Mishra, U., Camill, P., Yu, Z., Palmtag, J., and  
554 Kuhry, P.: Estimated stocks of circumpolar permafrost carbon with quantified uncertainty ranges and identified data  
555 gaps, *Biogeosciences*, 11, 6573-6593, 2014.
- 556 Jansson, P.-E. and Halldin, S.: Model for the annual water and energy flow in a layered soil, Comparison of forest  
557 and energy exchange models, *Society for Ecol. Model.*, Copenhagen, 145-163, 1979.
- 558 Jansson, P.-E. and Karlberg, L.: Coupled heat and mass transfer model for soil-plant-atmosphere systems, Royal  
559 Institute of Technology, Stockholm, 484 pp., available at: <http://www.coupmodel.com/documentation>, 2010.
- 560 Jansson, P. E.: CoupModel: Model Use, Calibration, and Validation, *Transactions of the ASABE*, 55, 1337, 2012.
- 561 Kersten, M. S.: Thermal properties of soils, *Bulletin*, 28, Minneapolis: Engineering Experiment Station, University of  
562 Minnesota, 1949.
- 563 Koven, C. D., Schuur, E. A. G., Schädel, C., Bohn, T. J., Burke, E. J., Chen, G., Chen, X., Ciais, P., Grosse, G.,  
564 Harden, J. W., Hayes, D. J., Hugelius, G., Jafarov, E. E., Krinner, G., Kuhry, P., Lawrence, D. M., MacDougall, A.  
565 H., Marchenko, S. S., McGuire, A. D., Natali, S. M., Nicolsky, D. J., Olefeldt, D., Peng, S., Romanovsky, V. E.,  
566 Schaefer, K. M., Strauss, J., Treat, C. C., and Turetsky, M.: A simplified, data-constrained approach to estimate the  
567 permafrost carbon-climate feedback, *Phil. Trans. R. Soc. A.*, 373, 20140423, [10.1098/rsta.2014.0423](https://doi.org/10.1098/rsta.2014.0423), 2015.
- 568 Lasslop, G., Reichstein, M., Papale, D., Richardson, A., Arneth, A., Barr, A., Stoy, P., and Wohlfahrt, G.:  
569 Separation of net ecosystem exchange into assimilation and respiration using a light response curve approach:  
570 critical issues and global evaluation, *Global Change Biol.*, 16, 187-208, 2010.
- 571 Li, J., Luo, Y., Natali, S., Schuur, E. A. G., Xia, J., Kowalczyk, E., and Wang, Y.: Modeling permafrost thaw and  
572 ecosystem carbon cycle under annual and seasonal warming at an Arctic tundra site in Alaska, *Journal of*  
573 *Geophysical Research: Biogeosciences*, 119, 1129-1146, 2014.
- 574 Lund, M., Falk, J. M., Friborg, T., Mbufong, H. N., Sigsgaard, C., Soegaard, H., and Tamstorf, M. P.: Trends in CO<sub>2</sub>  
575 exchange in a high Arctic tundra heath, 2000-2010, *Journal of Geophysical Research: Biogeosciences*, 117, 2012.
- 576 MacDougall, A. H., Avis, C. A., and Weaver, A. J.: Significant contribution to climate warming from the permafrost  
577 carbon feedback, *Nat. Geosci.*, 5, 719-721, 2012.
- 578 McGuire, A. D., Christensen, T. R., Hayes, D., Heroult, A., Euskirchen, E., Kimball, J. S., Koven, C., Lafleur, P.,  
579 Miller, P. A., Oechel, W., Peylin, P., Williams, M., and Yi, Y.: An assessment of the carbon balance of Arctic



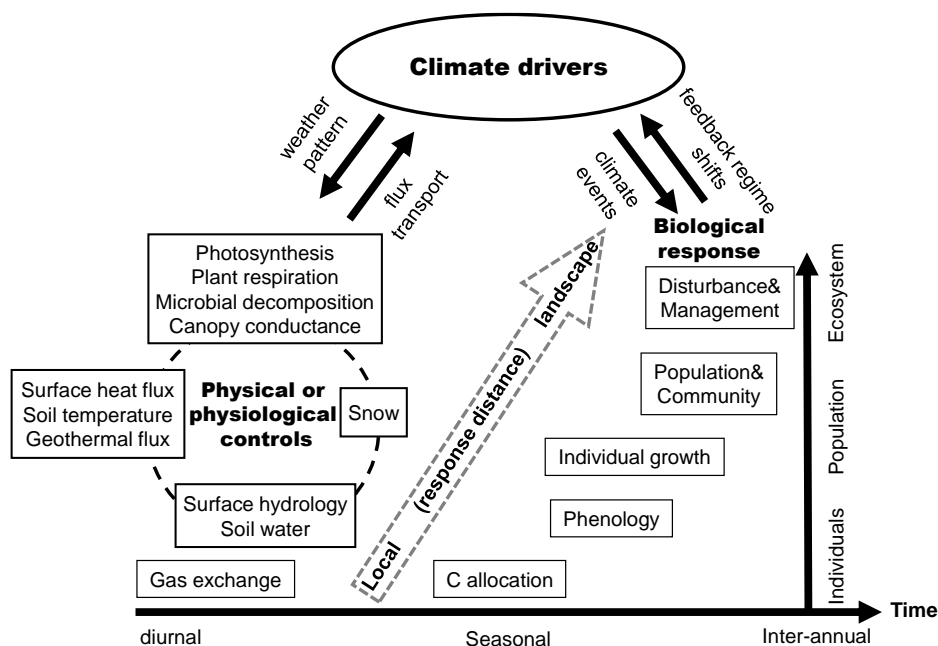
- 580 tundra: comparisons among observations, process models, and atmospheric inversions, *Biogeosciences*, 9, 3185-  
581 3204, 10.5194/bg-9-3185-2012, 2012.
- 582 Mellander, P.-E., Bergh, J., Lundmark, T., and Bishop, K.: Recovery of photosynthetic capacity in Scots pine: a  
583 model analysis of forest plots with contrasting soil temperature, *European Journal of Forest Research*, 127, 71-79,  
584 2008.
- 585 Molau, U.: Responses to natural climatic variation and experimental warming in two tundra plant species with  
586 contrasting life forms: *Cassiope tetragona* and *Ranunculus nivalis*, *Global Change Biology*, 3, 97-107, 1997.
- 587 Monteith, J. L.: Solar Radiation and Productivity in Tropical Ecosystems, *J. Appl. Ecol.*, 9, 747-766, 1972.
- 588 Monteith, J. L., and Moss, C. J.: Climate and the Efficiency of Crop Production in Britain [and Discussion], *Phil.*  
589 *Trans. R. Soc. A.*, 281, 277-294, 1977.
- 590 Myers-Smith, I. H., Elmendorf, S. C., Beck, P. S. A., Wilkening, M., Hallinger, M., Blok, D., Tape, K. D., Rayback,  
591 S. A., Macias-Fauria, M., Forbes, B. C., Speed, J. D. M., Boulanger-Lapointe, N., Rixen, C., Levesque, E., Schmidt,  
592 N. M., Baittinger, C., Trant, A. J., Hermanutz, L., Collier, L. S., Dawes, M. A., Lantz, T. C., Weijers, S., Jorgensen,  
593 R. H., Buchwal, A., Buras, A., Naito, A. T., Ravolainen, V., Schaepman-Strub, G., Wheeler, J. A., Wipf, S., Guay,  
594 K. C., Hik, D. S., and Vellend, M.: Climate sensitivity of shrub growth across the tundra biome, *Nat. Clim. Change*,  
595 5, 887-891, 2015.
- 596 Mäkelä, A., Hari, P., Berninger, F., Hänninen, H., Nikinmaa, E.: Acclimation of photosynthesis capacity in Scots  
597 pine to the annual cycle temperature, *Tree Physiol.*, 24, 369-378, 2004.
- 598 Natali, S. M., Schuur, E. A. G., Mauritz, M., Schade, J. D., Celis, G., Crummer, K. G., Johnston, C., Krapek, J.,  
599 Pegoraro, E., Salmon, V. G., and Webb, E. E.: Permafrost thaw and soil moisture driving CO<sub>2</sub> and CH<sub>4</sub> release from  
600 upland tundra, *Journal of Geophysical Research: Biogeosciences*, 120, 525-537, 10.1002/2014JG002872, 2015.
- 601 Paschalis, A., Fatichi, S., Katul, G. G., and Ivanov, V. Y.: Cross-scale impact of climate temporal variability on  
602 ecosystem water and carbon fluxes, *Journal of Geophysical Research: Biogeosciences*, 120, 1716-1740,  
603 10.1002/2015JG003002, 2015.
- 604 Prihodko, L., Denning, A. S., Hanan, N. P., Baker, I., and Davis, K.: Sensitivity, uncertainty and time dependence of  
605 parameters in a complex land surface model, *Agric. For. Meteorol.*, 148, 268-287, 2008.
- 606 Ratkowsky, D. A., Olley, J., McMeekin, T. A., and Ball, A.: Relationship between temperature and growth rate of  
607 bacterial cultures, *J. Bacteriol.*, 149, 1-5, 1982.
- 608 Reichstein, M., Falge, E., Baldocchi, D., Papale, D., Aubinet, M., Berbigier, P., Bernhofer, C., Buchmann, N.,  
609 Gilmanov, T., Granier, A., Grünwald, T., Havránková, K., Ilvesniemi, H., Janous, D., Knohl, A., Laurila, T., Lohila,  
610 A., Loustau, D., Matteucci, G., Meyers, T., Miglietta, F., Ourcival, J.-M., Pumpanen, J., Rambal, S., Rotenberg, E.,  
611 Sanz, M., Tenhunen, J., Seufert, G., Vaccari, F., Vesala, T., Yakir, D., and Valentini, R.: On the separation of net  
612 ecosystem exchange into assimilation and ecosystem respiration: review and improved algorithm, *Glob. Chang.*  
613 *Biol.*, 11, 2005.



- 614 Richardson, A. D., Hollinger, D. Y., Aber, J. D., Ollinger, S. V., and Braswell, B. H.: Environmental variation is  
615 directly responsible for short- but not long-term variation in forest-atmosphere carbon exchange, *Glob. Chang. Biol.*,  
616 13, 788-803, 2007.
- 617 Richardson, A. D., Mahecha, M. D., Falge, E., Kattge, J., Moffat, A. M., Papale, D., Reichstein, M., Stauch, V. J.,  
618 Braswell, B. H., Churkina, G., Kruijt, B., and Hollinger, D. Y.: Statistical properties of random CO<sub>2</sub> flux  
619 measurement uncertainty inferred from model residuals, *Agric. and For. Meteorol.*, 148, 38-50, 2008.
- 620 Schuur, E. A. G., Vogel, J. G., Crummer, K. G., Lee, H., Sickman, J. O., and Osterkamp, T. E.: The effect of  
621 permafrost thaw on old carbon release and net carbon exchange from tundra, *Nature*, 459, 556-559, 2009.
- 622 Schuur, E. A. G., McGuire, A. D., Schadel, C., Grosse, G., Harden, J. W., Hayes, D. J., Hugelius, G., Koven, C. D.,  
623 Kuhry, P., Lawrence, D. M., Natali, S. M., Olefeldt, D., Romanovsky, V. E., Schaefer, K., Turetsky, M. R., Treat, C.  
624 C., and Vonk, J. E.: Climate change and the permafrost carbon feedback, *Nature*, 520, 171-179, 2015.
- 625 Semenchuk, P. R., Christiansen, C. T., Grogan, P., Elberling, B., and Cooper, E. J.: Long-term experimentally  
626 deepened snow decreases growing-season respiration in a low- and high-Arctic tundra ecosystem, *J. Geophys. Res.:*  
627 *Biogeosci.*, 121, 1236-1248, 2016.
- 628 Skopp, J., Jawson, M. D., and Doran, J. W.: Steady-State Aerobic Microbial Activity as a Function of Soil Water  
629 Content, *Soil Sci. Soc. Am. J.*, 54, 1619-1625, 1990.
- 630 Stoy, P. C., Katul, G. G., Siqueira, M. B. S., Juang, J.-Y., McCarthy, H. R., Kim, H.-S., Oishi, A. C., and Oren, R.:  
631 Variability in net ecosystem exchange from hourly to inter-annual time scales at adjacent pine and hardwood forests:  
632 a wavelet analysis, *Tree Physiol.*, 25, 887-902, 2005
- 633 Stoy, P. C., Richardson, A. D., Baldocchi, D. D., Katul, G. G., Stanovick, J., Mahecha, M. D., Reichstein, M., Detto,  
634 M., Law, B. E., Wohlfahrt, G., Arriga, N., Campos, J., McCaughey, J. H., Montagnani, L., Paw U, K. T., Sevanto,  
635 S., and Williams, M.: Biosphere-atmosphere exchange of CO<sub>2</sub> in relation to climate: a cross-biome analysis across  
636 multiple time scales, *Biogeosciences*, 6, 2297-2312, 2009.
- 637 Stoy, P. C., Dietze, M. C., Richardson, A. D., Vargas, R., Barr, A. G., Anderson, R. S., Arain, M. A., Baker, I. T.,  
638 Black, T. A., Chen, J. M., Cook, R. B., Gough, C. M., Grant, R. F., Hollinger, D. Y., Izaurralde, R. C., Kucharik, C.  
639 J., Lafleur, P., Law, B. E., Liu, S., Lokupitiya, E., Luo, Y., Munger, J. W., Peng, C., Poulter, B., Price, D. T.,  
640 Ricciuto, D. M., Riley, W. J., Sahoo, A. K., Schaefer, K., Schwalm, C. R., Tian, H., Verbeeck, H., and Weng, E.:  
641 Evaluating the agreement between measurements and models of net ecosystem exchange at different times and time  
642 scales using wavelet coherence: an example using data from the North American Carbon Program Site-Level  
643 Interim Synthesis, *Biogeosciences*, 10, 2013.
- 644 Vargas, R., Detto, M., Baldocchi, D. D., and Allen, M. F.: Multiscale analysis of temporal variability of soil CO<sub>2</sub>  
645 production as influenced by weather and vegetation, *Glob. Chang. Biol.*, 16, 1589-1605, 10.1111/j.1365-  
646 2486.2009.02111.x, 2010.

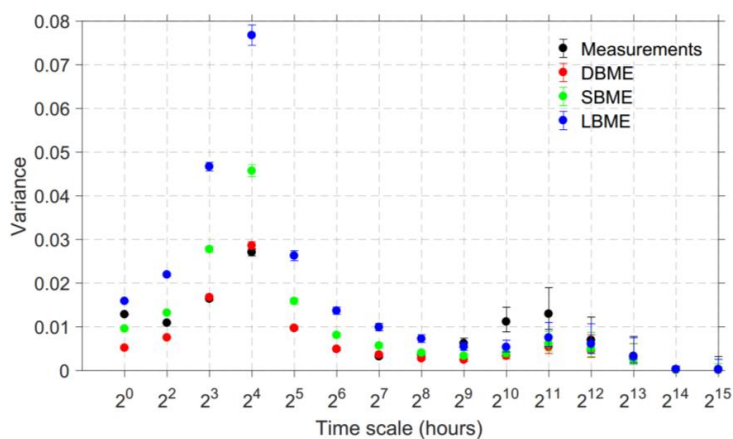


- 647 Webb, E. E., Schuur, E. A. G., Natali, S. M., Oken, K. L., Bracho, R., Krapek, J. P., Risk, D., and Nickerson, N. R.:  
648 Increased wintertime CO<sub>2</sub> loss as a result of sustained tundra warming, *J. Geophys. Res.: Biogeosci.*, 121, 249-265,  
649 2016.
- 650 Westergaard-Nielsen, A., Lund, M., Pedersen, S. H., Schmidt, N. M., Klosterman, S., Abermann, J., and Hansen, B.  
651 U.: Transitions in high-Arctic vegetation growth patterns and ecosystem productivity tracked with automated  
652 cameras from 2000 to 2013, *AMBIO*, 46, 39-52, 2017.
- 653 Wetterstedt, J. Å. M., and Ågren, G. I.: Quality or decomposer efficiency – which is most important in the  
654 temperature response of litter decomposition? A modelling study using the GLUE methodology, *Biogeosciences*, 8,  
655 477-487, 10.5194/bg-8-477-2011, 2011.
- 656 Williams, M., Richardson, A. D., Reichstein, M., Stoy, P. C., Peylin, P., Verbeeck, H., Carvalhais, N., Jung, M.,  
657 Hollinger, D. Y., Kattge, J., Leuning, R., Luo, Y., Tomelleri, E., Trudinger, C. M., and Wang, Y. P.: Improving land  
658 surface models with FLUXNET data, *Biogeosciences*, 6, 1341-1359, 2009.
- 659 Wu, J., van der Linden, L., Lasslop, G., Carvalhais, N., Pilegaard, K., Beier, C., and Ibrom, A.: Effects of climate  
660 variability and functional changes on the inter-annual variation of the carbon balance in a temperate deciduous  
661 forest, *Biogeosciences*, 9, 13-28, 2012a.
- 662 Wu, J., Guan, K., Hayek, M., Restrepo-Coupe, N., Wiedemann, K. T., Xu, X., Wehr, R., Christoffersen, B. O.,  
663 Miao, G., da Silva, R., de Araujo, A. C., Oliveira, R. C., Camargo, P. B., Monson, R. K., Huete, A. R., and Saleska,  
664 S. R.: Partitioning controls on Amazon forest photosynthesis between environmental and biotic factors at hourly to  
665 inter-annual time scales, *Glob. Chang. Biol.*, 23, 1240-1257, 2017.
- 666 Wu, S. H., Jansson, P.-E., and Kolari, P.: The role of air and soil temperature in the seasonality of photosynthesis  
667 and transpiration in a boreal Scots pine ecosystem, *Agric. For. Meteorol.*, 156, 85-103, 2012b.
- 668 Xia, J., McGuire, A. D., Lawrence, D., Burke, E., Chen, G., Chen, X., Delire, C., Koven, C., MacDougall, A., Peng,  
669 S., Rinke, A., Saito, K., Zhang, W., Alkama, R., Bohn, T. J., Ciais, P., Decharme, B., Gouttevin, I., Hajima, T.,  
670 Hayes, D. J., Huang, K., Ji, D., Krinner, G., Lettenmaier, D. P., Miller, P. A., Moore, J. C., Smith, B., Sueyoshi, T.,  
671 Shi, Z., Yan, L., Liang, J., Jiang, L., Zhang, Q., and Luo, Y.: Terrestrial ecosystem model performance in simulating  
672 productivity and its vulnerability to climate change in the northern permafrost region, *J. Geophys. Res.: Biogeosci.*,  
673 122, 430-446, 2017.
- 674 Zhang, W., Miller, P. A., Smith, B., Wania, R., Koenigk, T., and Döscher, R.: Tundra shrubification and tree-line  
675 advance amplify Arctic climate warming: results from an individual-based dynamic vegetation model, *Environ. Res.  
676 Lett.*, 8, 034023, 2013a.
- 677 Zhang, W., Jansson, C., Miller, P. A., Smith, B., and Samuelsson, P.: Biogeophysical feedbacks enhance the Arctic  
678 terrestrial carbon sink in regional Earth system dynamics, *Biogeosciences*, 11, 5503-5519, 2014.
- 679 Zhang, X., He, J., Zhang, J., Polyakov, I., Gerdes, R., Inoue, J., and Wu, P.: Enhanced poleward moisture transport  
680 and amplified northern high-latitude wetting trend, *Nat. Clim. Change*, 3, 47-51, 2013b.



681  
 682  
 683  
 684  
 685  
 686  
 687  
 688  
 689

Figure 1. Physical/physiological controls and biological responses operated at different temporal (x axis) and ecosystem-level (y axis) scale by process-based ecosystem models.



690

691

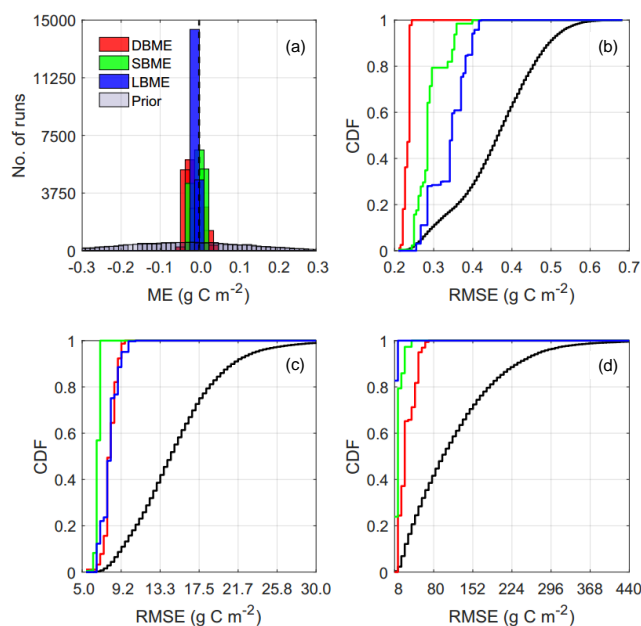
692

693

**Figure 2. Variance of Maximum Overlap Discrete Wavelet Transform for net ecosystem exchange of the measurements (black) and model ensembles means - DBME (red), SBME (green) and LBME (blue). DBME, SBME and LBME refer to the diurnal, seasonal and long-term behaviour model ensemble respectively.**

694

695



696

697

698

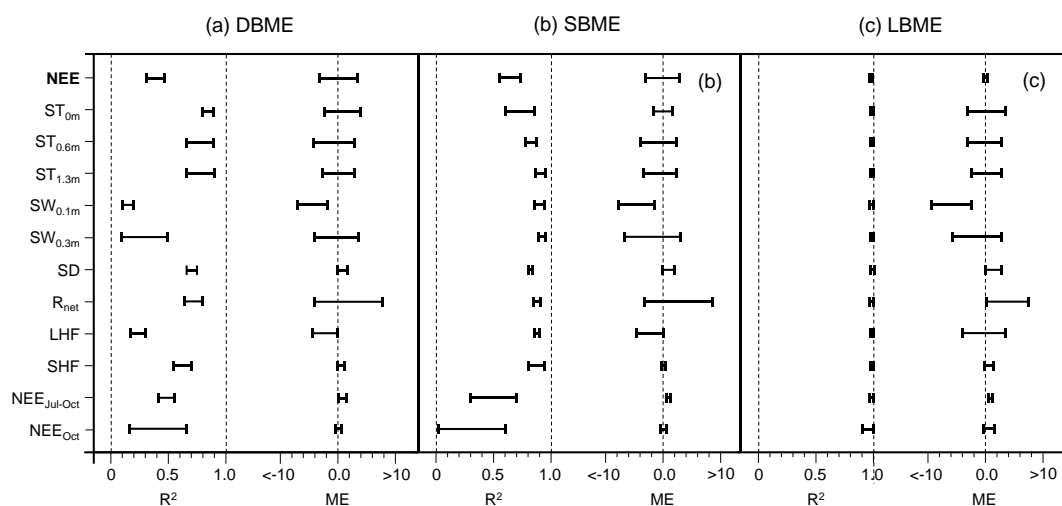
699

700

701

**Figure 3.** (a) The number of runs in mean errors (ME) of NEE flux ( $\text{g C m}^{-2}$ ). (b) Cumulative distribution of frequency (CDF) in root mean square errors (RMSE,  $\text{g C m}^{-2}$ ) for the daily-integrated NEE flux. (c) CDF in RMSE ( $\text{g C m}^{-2}$ ) for the yearly-integrated NEE flux. (d) CDF in RMSE ( $\text{g C m}^{-2}$ ) for the entire period-integrated NEE flux. The colour type denotes the prior runs (black), the diurnal behaviour model ensemble (DBME, red), the seasonal behaviour model ensemble (SBME, green) and the long-term behaviour model ensemble (LBME, blue).

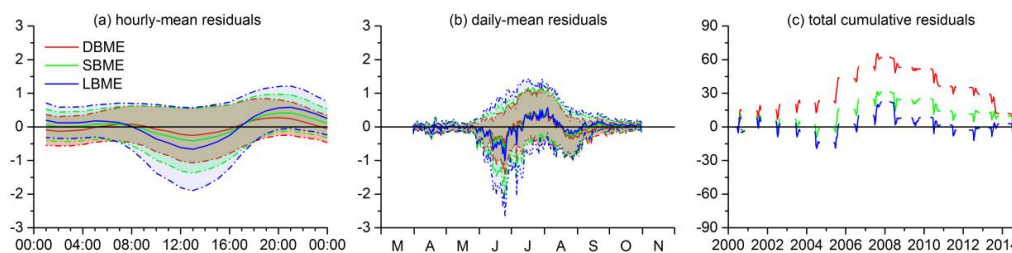
702



703

704 **Figure 4.** The coefficient of determination for linear regression ( $R^2$ ) and mean errors (MR) for the behaviour model  
 705 ensembles in simulating the measurement variables: net ecosystem exchange (NEE,  $\text{g m}^{-2} \text{d}^{-1}$ ), soil temperature for the  
 706 surface and the depth of 0.6 and 1.3 m ( $ST_{0m}$ ,  $ST_{0.6m}$  and  $ST_{1.3m}$ ,  $^{\circ}\text{C}$ ), soil water content at the depth of 0.1 m and 0.3 m  
 707 ( $SW_{0.1m}$  and  $SW_{0.3m}$ , %), snow depth (SD, m), net radiation flux ( $R_{net}$ ,  $\text{J m}^{-2} \text{d}^{-1}$ ), latent heat flux (LHF,  $\text{J m}^{-2} \text{d}^{-1}$ ), sensible  
 708 heat flux (SHF,  $\text{J m}^{-2} \text{d}^{-1}$ ), net ecosystem exchange for July to October ( $NEE_{Jul-Oct}$ ,  $\text{g m}^{-2} \text{d}^{-1}$ ) and net ecosystem exchange  
 709 for October ( $NEE_{Oct}$ ,  $\text{g m}^{-2} \text{d}^{-1}$ ). The behaviour models are constrained using (a) the daily-integrated NEE (DBME), (b)  
 710 the yearly-integrated NEE (SBME) and (c) the entire period-integrated NEE (LBME). The error bar indicates the range  
 711 of maximum and minimum values of  $R^2$ /MR for the behaviour ensembles. Note that the range of MR for the variables of  
 712 NEE,  $R_{net}$ , LHF, SHF,  $NEE_{Jul-Oct}$  and  $NEE_{Oct}$  has been scaled to [-10, 10], so their original ranges can be attained by  
 713 multiplying the factors  $1 \times 10^{-2}$ ,  $1 \times 10^5$ ,  $1 \times 10^5$ ,  $1 \times 10^6$ ,  $1 \times 10^{-2}$  and  $1 \times 10^{-2}$  respectively.

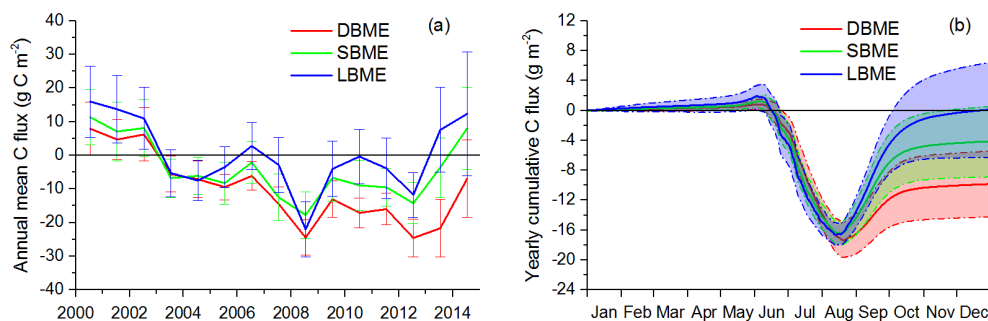
714



715

716 **Figure 5. The residuals ( $\text{g C m}^{-2}$ ) between each model ensemble mean and measurements for the period 2000-2014. The**  
 717 **model ensembles are DBME – the diurnal behaviour model ensemble (red), SBME – the seasonal behaviour model**  
 718 **ensemble (green) and LBME – the long-term behaviour model ensemble (blue). (a) Hourly mean residuals ( $\text{g C m}^{-2}$ ). (b)**  
 719 **Daily mean residuals ( $\text{g C m}^{-2}$ ). (c) Total cumulated residuals ( $\text{g C m}^{-2}$ ).**

720



721

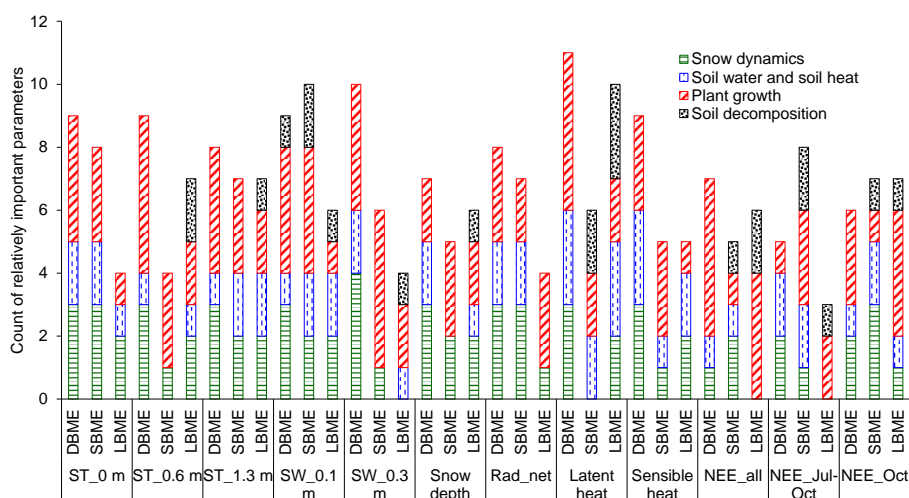
722

723

724

**Figure 6. The annual mean C flux (a) and yearly cumulated C flux (b) for three model ensembles. The model ensembles are the diurnal behaviour model ensemble (DBME, red), the seasonal behaviour model ensemble (SBME, green) and the long-term behaviour model ensemble (LBME, blue).**

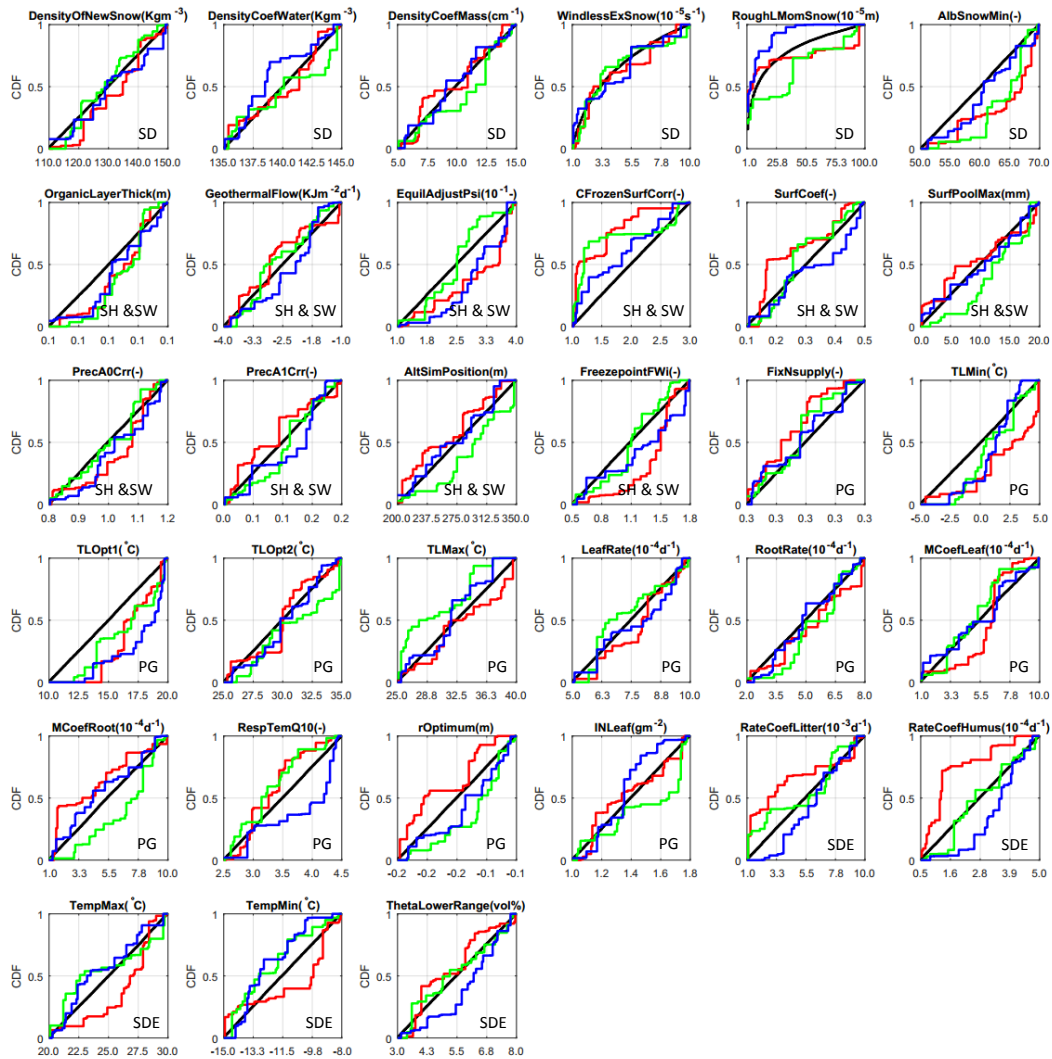
725



726

727 **Figure 7.** Count of parameters with Pearson correlation coefficient ( $r > 0.3$  or  $r < -0.3$ ) against model performance with  
 728 coefficient of determination ( $R^2$ ) in measurement variables (i.e. surface temperature ( $ST_{0m}$ ), soil temperature at the depth  
 729 of 0.6m ( $ST_{0.6m}$ ), soil temperature at the depth of 1.3 m ( $ST_{1.3m}$ ), soil water content at the depth of 0.1 m ( $SW_{0.1m}$ ), soil  
 730 water content at the depth of 0.3 m ( $SW_{0.3m}$ ), Snow depth (SD), net radiation flux ( $R_{net}$ ), latent heat flux (LHF), sensible  
 731 heat flux (SHF), NEE flux for the entire measurement period (NEE), NEE flux for July-October (NEE<sub>J-O</sub>), NEE flux for  
 732 October (NEE<sub>Oct</sub>).

733



734

735

736

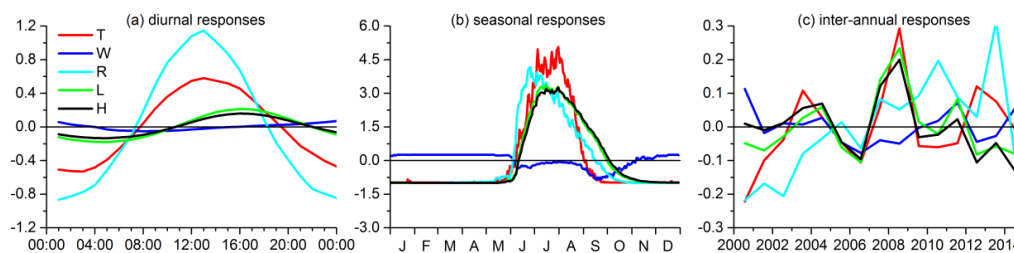
737

738

739

**Figure 8.** Cumulative distribution frequency (CDF) of all the sampled parameters in the prior runs (black) and posterior runs (the diurnal behaviour model ensemble - red, the seasonal behaviour model ensemble - green and the long-term behaviour model ensemble - blue). The definition of the parameters is given in Table S1. These parameters regulate the processes of snow dynamics (SD), soil heat and soil water transfer (SH & SW), plant growth (PG) and soil decomposition (SDE).

740



741

742

743

744

745

746

**Figure 9.** The normalized anomalies of ecosystem responses to total photosynthesis and ecosystem respiration at the diurnal (only accounting for the growing season, May-Oct.), seasonal and inter-annual scales. Ecosystem responses shown here are the air temperature response of total photosynthesis (T – red), the water stress response of total photosynthesis (W – blue), the absorbed radiation (R – cyan), the soil litter respiration response (L – green) and the soil humus respiration response (H – black).

747

748 **Table 1. Site characteristics of *Cassiope tetragona* heath tundra ecosystem at Zackenberg.**

	Zackenberg	References
<b>Climate characteristics</b>		
Air Temperature (annual) (°C) & linear trend (°C yr <sup>-1</sup> )	-9.19 & 0.06 for 1996-2014	GEM database <sup>1</sup>
Air Temperature (JJA) (°C) & linear trend (°C yr <sup>-1</sup> )	-4.65 & 0.09 for 1996-2014	GEM database
Air Temperature (DJF) (°C) & linear trend (°C yr <sup>-1</sup> )	-19.07 & 0.15 for 1996-2014	GEM database
Precipitation (annual) (mm) & linear trend (mm yr <sup>-1</sup> )	219 & 4 for 1996-2014	GEM database
Snow depth (max.) (m) & linear trend (cm yr <sup>-1</sup> )	78 & -1.9 for 1997-2014	GEM database
<b>Plant characteristics</b>		
Woody species (degree of cover):		
<i>Cassiope Tetragona</i>	53%	Bay 1998
<i>Salix Arctica</i>	3%	Bay 1998
<i>Dryas</i>	<1%	Bay 1998
Total of herbs	<1%	Bay 1998
Total of mosses	8%	Bay 1998
Total of lichens	3%	Bay 1998
Life-span of leaves (yr)	3 - 10	Molau 1997
Averaged shrub height (cm)	5 - 10	Elberling et al., 2008; Campioli et al., 2012
Leaf area index (m <sup>2</sup> leaves m <sup>-2</sup> ground)	0.4 - 0.5	Campioli et al., 2009
Albedo (-)		
summer	0.15 - 0.8	Hanssen et al., 2008
winter		
Leaf biomass (g m <sup>-2</sup> )	95 <sup>a</sup> or 60 <sup>b</sup>	
Stem biomass (g m <sup>-2</sup> )	518 <sup>a</sup> or 400 <sup>b</sup>	<sup>a</sup> Elberling et al., 2008;
Root biomass (g m <sup>-2</sup> )	250 <sup>a</sup> g m <sup>-2</sup>	<sup>b</sup> Arndal et al., 2009
Moss biomass (g m <sup>-2</sup> )	235 <sup>a</sup> or 120 <sup>b</sup> g m <sup>-2</sup>	
Leaf nitrogen (g m <sup>-2</sup> )	1 g m <sup>-2</sup>	Arndal et al., 2009
Above-ground C:N ratio (-)	60	Elberling et al., 2008
<b>Soil characteristics</b>		
Soil type	<i>Typic Psammenturbels</i>	Elberling&Jakobsen, 2000
Soil bulk density (g cm <sup>-3</sup> )	0.8-1.6	Elberling et al., 2004
Water saturation at 0-5 cm (%)	60-80	Elberling et al., 2004
Soil pH	5.0-7.2	Elberling et al., 2004
Soil carbon content at 0-20 cm / 0-50 cm (kg C m <sup>-2</sup> )	6.3 (± 3.0) / 8.5 (± 2.6)	Elberling et al., 2004
Soil C:N ratio (-) at 0-5 cm/ 17-22 cm/ > 22 cm	16.2/17.3/20.4	Elberling et al., 2004
NO <sub>3</sub> -N (ppm) at 5 cm/10 cm/30 cm	0.9/0.4/2.0	Elberling et al., 2004
NH <sub>4</sub> -N (ppb) at 5 cm/10 cm/30 cm	15.8/11.7/11.7	Elberling et al., 2004

749 <sup>1</sup>Greenland Ecosystem Monitoring Database, <http://data.g-e-m.dk/>



750 Table 2. The minimum and maximum parameter values in the prior runs. The mean (Mean), coefficient of variation (CV), the standard deviation divided by the mean),  
 751 skewness (S) and kurtosis (K) of probability density functions of parameter values in the posterior runs (around 30 runs). The definition of parameters and the relevant  
 752 equations are given in the Table S1.

Parameters	Unit	Equation	Prior		DBME Posterior (34 runs)					SBME Posterior (31 runs)					LBME Posterior (29 runs)				
			Min	Max	Mean	CV	S	K	Mean	CV	S	K	Mean	CV	S	K	Mean	CV	S
<i>Snow dynamics</i>																			
DensityOfNewSnow	Kg m <sup>-3</sup>	Eqn. S1	110	150	134.5	0.09	-0.54	-0.78	133.99	0.08	-0.2	-0.91	131.93	0.08	-0.13	-0.93			
DensityCofWater	Kg m <sup>-3</sup>	Eqn. S1	135	145	140.03	0.02	-0.09	-1.38	139.97	0.02	0	-1.59	140.06	0.02	-0.04	-1.49			
DensityCofMass	m <sup>-1</sup>	Eqn. S1	0.05	0.15	0.1	0.31	0.15	-1.55	0.11	0.29	-0.17	-1.55	0.1	0.36	0.29	-1.31			
WindlessExSnow	s <sup>-1</sup>	Eqn. S2	e-05	e-04	3.88e-05	0.65	0.78	-0.56	4.7e-05	0.62	0.66	-0.85	4e-05	0.6	0.77	-0.04			
RoughLMonSnow	m	Eqn. S3	e-05	e-03	2.35e-04	1.27	1.47	0.9	3.28e-04	0.98	0.62	-1.02	1.3e-04	1.17	1.7	2.19			
AlbSnowMin	%	Eqn. S4	50	70	63.59	0.09	-0.78	-0.32	63.52	0.08	-0.91	0.18	61.41	0.09	-0.07	-0.58			
<i>Soil heat and soil water</i>																			
OrganicLayerThick	m	Eqn. S6	0.06	0.1	0.08	0.13	-0.5	-0.78	0.08	0.09	-0.66	0.14	0.08	0.15	-0.08	-1.03			
GeothermalFlow	J m <sup>-2</sup> d <sup>-1</sup>	-	-4e03	-1000	-2559	0.33	0.31	-0.96	-2353	0.33	-0.06	-1.27	-2376	0.39	-0.31	-1.35			
EquilAdjustPsi	-	Eqn. S7	1	3	1.48	0.37	1.4	1.3	1.69	0.44	0.6	-1.51	1.92	0.31	0.21	-1.15			
CFrozenSurfCorr	-	Eqn. S8	0.1	0.4	0.26	0.35	-0.16	-1.44	0.24	0.36	0.23	-0.76	0.27	0.32	0.4	-0.84			
SurfCofef	mm	Eqn. S9	0.1	0.5	0.28	0.42	0.4	-1.4	0.32	0.37	-0.11	-1.41	0.31	0.38	0.07	-1.02			
SurfPoolMax	mm	Eqn. S9	0	20	9.99	0.6	-0.17	-1.08	11.82	0.43	-0.49	-0.81	10.9	0.57	-0.45	-1.01			
PrecAOCrr	-	Eqn. S10	0.8	1.2	1.01	0.11	-0.32	-1.06	0.98	0.11	0.34	-0.85	1.02	0.11	-0.1	-1.14			
PrecAICrr	-	Eqn. S10	0	0.2	0.09	0.69	0.23	-1.32	0.09	0.67	0.19	-1.27	0.11	0.55	-0.26	-1.4			
AlbSimPosition	-	-	200	350	269.21	0.16	-0.16	-1.23	283.03	0.15	-0.4	-0.58	271.86	0.16	-0.09	-1.27			
FreezepointFWi	-	Eqn. S11	0.5	1.8	1.23	0.28	-0.33	-0.93	1.17	0.31	-0.43	-0.96	1.27	0.32	-0.33	-1.13			
<i>Plant growth</i>																			



FixNsupply	-	Eqn. S12	0.31	0.35	0.32	0.03	0.5	-1.03	0.33	0.03	0.25	-0.93	0.33	0.04	-0.08	-1.27
TLMin	°C	Eqn. S13	-5	5	2.24	1.16	-1.06	0.2	1.22	1.89	0.15	-1.39	1.14	1.73	-0.37	-0.46
TLOpt1	°C	Eqn. S13	10	20	17.61	0.1	-0.38	-0.9	16.6	0.16	-0.4	-1.29	17.94	0.11	-1.23	0.46
TLOpt2	°C	Eqn. S13	25	35	29.8	0.1	-0.04	-1.21	30.81	0.09	-0.01	-1.46	30.66	0.09	-0.37	-0.74
TLMax	°C	Eqn. S13	25	40	32.1	0.14	0.09	-1.16	28.3	0.13	1.28	0.45	31.33	0.11	0.09	-0.54
LeafRate	-	Eqn. S14	5e-4	e-3	8.16e-04	0.16	-0.49	-0.62	7.81e-04	0.17	0.14	-1.19	7.98e-04	0.19	-0.67	-0.79
RootRate	-	Eqn. S14	2e-4	8e-4	4.74e-04	0.37	0.12	-0.97	5.22e-04	0.31	0.07	-1	4.88e-04	0.35	0.2	-1.31
MCoefLeaf	d <sup>-1</sup>	Eqn. S15	-0.2	-0.13	5.15e-04	0.51	0.11	-1.04	6.77e-04	0.35	-0.63	-0.59	5.71e-04	0.51	-0.09	-1.49
MCoefRoot	d <sup>-1</sup>	Eqn. S15	e-4	0.001	5.61e-04	0.43	-0.43	-0.51	5.2e-04	0.47	0.13	-0.42	5.58e-04	0.49	-0.37	-0.97
RespTempQ10	-	Eqn. S16	2.5	4.5	3.45	0.17	0.27	-1.08	3.31	0.17	0.26	-0.87	3.67	0.17	0.22	-1.44
rOptimum	m	-	e-04	0.001	-0.17	0.11	0.29	-1.51	-0.16	0.13	-0.47	-1.08	-0.16	0.12	-0.28	-1.24
INLeaf	g	-	1	1.8	1.39	0.15	0.31	-0.78	1.43	0.19	-0.1	-1.58	1.39	0.14	-0.09	-0.57
<i>Soil decomposition</i>																
RateCofLitter	d <sup>-1</sup>	Eqn. S17	e-3	0.01	3.86e-03	0.73	0.86	-0.65	5.63e-03	0.49	-0.4	-1.29	5.74e-03	0.38	0.14	-1.18
RateCofHumus	d <sup>-1</sup>	Eqn. S18	5e-5	5e-4	1.61e-04	0.72	1.07	-0.19	2.88e-04	0.43	-0.02	-0.82	3.43e-04	0.31	-0.98	0.36
TempMax	°C	Eqn. S19	20	30	26.43	0.09	-1.11	0.7	25.41	0.12	-0.12	-1.39	24.01	0.11	0.4	-0.92
TempMin	°C	Eqn. S19	-15	-8	-11.28	0.22	-0.15	-1.67	-11.5	0.16	0.32	-0.78	-12.35	0.13	-0.67	-0.78
ThetaLowerRange	Vol %	Eqn. S20	3	8	5.62	0.25	-0.04	-1.38	5.7	0.24	-0.13	-1.12	5.83	0.22	-0.49	-0.71



**Table 3. The acceptance criteria used to constrain a 19,000 Monte-Carlo multi-run for three behaviour model ensembles.**

Ensemble	Variables	Root mean square error (g C m <sup>-2</sup> )	Mean Error (g C m <sup>-2</sup> )	No. of accepted runs
		$\sqrt{\frac{1}{n} \sum_{i=1}^n (\text{Model}_i - \text{Obs}_i)^2}$	$\frac{1}{n} \sum_{i=1}^n (\text{Model}_i - \text{Obs}_i)$	
DBME	Daily cumulative NEE	≤ 0.24	(-0.04, 0.04)	34
SBME	Yearly cumulative NEE	≤ 7.16	(-0.02, 0.02)	31
LBME	Long-term cumulative NEE	≤ 15.07	(-0.008, 0.008)	29



**Table 4. The mean C budget simulated by the three model behaviour ensembles (DBME – diurnal behaviour model ensemble, SBME – seasonal behaviour model ensemble and LBME – long-term behaviour model ensemble). The bold type indicates the slope of linear trend with  $p < 0.05$ .**

	DBME (2000-2014)		SBME (2000-2014)		LBME (2000-2014)	
	mean (g C m <sup>-2</sup> yr <sup>-1</sup> )	slope of linear trend	mean (g C m <sup>-2</sup> yr <sup>-1</sup> )	slope of linear trend	mean (g C m <sup>-2</sup> yr <sup>-1</sup> )	slope of linear trend
NEE	-9.8 ± 10.4	<b>-1.83</b>	-4.1 ± 8.9	-0.83	-0.1 ± 10.5	-0.62
GPP	-59.4 ± 16.1	<b>-2.76</b>	-79.9 ± 15.7	-1.26	-99.5 ± 19	0.79
ER	49.6 ± 6.4	<b>0.93</b>	75.8 ± 8.3	0.44	99.7 ± 9.8	0.16
R <sub>soil</sub>	41.3 ± 4.4	0.48	63.6 ± 6.5	0.14	84.5 ± 7.6	-0.12
R <sub>plant</sub>	24.4 ± 6.8	<b>1.28</b>	22.5 ± 4.3	<b>0.55</b>	27.1 ± 4.9	0.44
R <sub>root</sub>	16.2 ± 4.5	<b>0.84</b>	10.4 ± 2	<b>0.25</b>	11.9 ± 2.1	0.16
R <sub>litter</sub>	24.8 ± 8.6	0.07	35.5 ± 3.6	0	44.4 ± 3.7	-0.01
R <sub>humus</sub>	8.6 ± 0.7	0.02	17.7 ± 1.7	-0.11	28.2 ± 2.6	-0.27
Litterfall <sub>leaves&amp;stem</sub>	12.6 ± 3.1	<b>0.69</b>	22 ± 4.5	<b>0.99</b>	28.2 ± 5.9	<b>1.29</b>
Litterfall <sub>root</sub>	15 ± 3.3	<b>0.74</b>	19.4 ± 4.4	<b>0.95</b>	24.3 ± 5	<b>1.07</b>
Humus <sub>form</sub>	4.8 ± 0.4	0.03	6.9 ± 0.7	<b>0.02</b>	8.8 ± 0.8	0.02
C <sub>leaf</sub>	145.9 ± 47.9	<b>10.67</b>	209.8 ± 49.5	<b>10.95</b>	262.9 ± 58.5	<b>12.86</b>
C <sub>stem</sub>	362.7 ± 6.2	<b>-1.37</b>	390.7 ± 0.7	0.02	398.9 ± 4.4	<b>0.96</b>
C <sub>root</sub>	94.6 ± 26.4	<b>5.86</b>	112.9 ± 23.6	<b>5.07</b>	155.6 ± 29.5	<b>6.31</b>
C <sub>moss</sub>	163.3 ± 47.6	<b>10.62</b>	126.4 ± 26.9	<b>5.96</b>	136.4 ± 23.3	<b>5.11</b>
C <sub>litter</sub>	1157.7 ± 18.3	-2.06	985.4 ± 18.9	-0.37	789.5 ± 21.6	0.07
C <sub>humus</sub>	9113.3 ± 17.2	<b>-3.84</b>	8958.5 ± 49.7	<b>-11.11</b>	8762.2 ± 88.3	<b>-19.75</b>
C <sub>som</sub>	10271.1 ± 30.8	<b>-5.91</b>	9943.9 ± 55.1	<b>-11.49</b>	9551.7 ± 91.2	<b>-19.67</b>